Supporting Information

The Shastry-Sutherland lattice in two-dimensional magnetic lanthanide metal-organic frameworks

Jing Li,[‡b] Xiao Sun,[‡a] Peiqiong Chen,[‡a] Ruiqin Huang,[d] Suyuan Zeng,[a] Hou-Ting Liu,[e] Yibo Han,*[d] Yi-Quan Zhang*[c] and Haiquan Tian*[a]

[a] Shandong Provincial Key Laboratory of Chemical Energy Storage and Novel Cell Technology, School of Chemistry and Chemical Engineering, Liaocheng University, Liaocheng 252059, P. R. China

[b] Division of Advanced Materials, and Vacuum Interconnected Nanotech Workstation, Suzhou Institute of Nano-Tech and Nano-Bionics, Chinese Academy of Sciences, Suzhou 215123, P. R. China

[c] Jiangsu Key Laboratory for NSLSCS, School of Physical Science and Technology, Normal University, Nanjing 210023, PR China

[d] Wuhan National High Magnetic Field Center & School of Physics, Huazhong University of Science and Technology, Wuhan 430074, P. R. China

[e] Food and Biochemistry Engineering Department, Yantai Vocational College, Yantai 264006, P. R. China

Table of Contents

S1 Experimental Section

Synthesis

All starting materials were of reagent grade were purchased from commercial suppliers and as received without further purification. All of the four compounds were performed under aerobic conditions.

Two-dimension 1:

For $DyCl_2(ppch)_{0.5}\cdot 2DMF$ (**1**): Solid **2** (0.0937 g, 0.8 mmol) was added to a stirred solution of $DyCl_3\cdot 6H_2O$ (0.1506 g, 0.4 mmol) in *N*, *N*-dimethylformamide (8.0 mL) at ambient temperature. The resulting mixture was stirred for a further 6 h, and then at 100 °C for 4 days. Yellow block-shaped crystals of **1**, suitable for X-ray diffraction analysis, were formed in 23% yield (15 mg, based on Dy). Elemental analysis calcd (%) for $C_{11}H_{17}DyN_5O_3Cl$: C, 28.39, H, 3.68, N, 15.05: found C, 27.01, H, 3.51, N, 15.36. IR (KBr, cm^{-1}): 3455-2623(br), 1671(vs), 1625(vs), 1606(s), 1559(vs), 1503(w), 1465(m), 1434(m), 1421(m), 1376(vs), 1287(w), 1423(m), 1198(m), 1153(s), 1108(s), 1063(m), 1025(s), 872(m), 769(m),745(m), 712(w), 687(s), 572(m), 489(m), 455(m), 424(w). Thermal analysis revealed that the weight loss below 210 °C was 16.4%, in line with the release of one DMF molecules (calcd. 15.9%).

Two-dimension 1-Y:

For $YCl_2(ppch)_{0.5}\cdot 2DMF$ (**1-Y**): The pale-yellow crystals were prepared using the same procedure as for **1** except that $YCl_3\cdot 6H_2O$ (0.0607 g, 0.2 mmol) was used as the starting material. Yield: 32 mg (35%, based on Y). Elemental analysis calcd (%) for $C_{11}H_{17}YN_5O_3Cl$: C, 33.73, H, 4.37, N, 17.88: found C, 32.51, H, 4.16, N, 18.22. IR (KBr, cm^{-1}): 3452-2609(br), 1662(vs), 1605(s), 1499(w), 1472(w), 1439(m), 1413(m), 1375(s), 1286(w), 1246(w), 1191(m), 1152(s), 1121(m), 1155(m), 1024(m), 877(m), 782(m), 749(m), 719(w), 673(s), 565(m), 495(m), 456(m). Thermal analysis revealed that the weight loss below 240 °C was 29.7%, in agreement with the release of two DMF molecules (calcd. 30.9%).

Two-dimension 1-$Dy_{0.50}Y_{0.50}$:

The site-substituted **1-$Dy_{0.50}Y_{0.50}$** sample was synthesized in accordance with the

synthesis of pure **1**, with an accurately measured 1:1 molar ratio of dysprosium(III) and yttrium(III) chloride starting materials. IR (KBr, cm-1): 3388-2719(br), 1669(s), 1605(s), 1548(vs), 1490(w), 1455(w), 1419(m), 1376(vs), 1318(w), 1282(w), 1225(m), 1189(m), 1161(s), 1118(w), 1060(m), 1025(s), 889(m), 767(w), 745(w), 703(w), 580(w), 523w), 548(m), 463(w).

Two-dimension 1-$Dy_{0.10}Y_{0.90}$:

The site-substituted **1-$Dy_{0.10}Y_{0.90}$** sample was synthesized in accordance with the synthesis of pure **1**, with an accurately measured 1:9 molar ratio of dysprosium(III) and yttrium(III) chloride starting materials. IR (KBr, cm-1): 3426-2956(br), 1665(s), 1615(s), 1544(vs), 1472(w), 1422(m), 1387(s), 1309(w), 1223(m), 1180(m), 1151(s), 1116(w), 1066(m), 1039(m), 880(m), 787(w), 745(w), 716(w), 581(w), 516(w), 460(w).

Dimer 2:

For $Dy_2Cl_2(ppch)(H_2pc)_2 \cdot 4MeOH$ (**2**): A mixture of pyrazine-2- carbohydrazide (H_3pc, 0.0600 g, 0.4 mmol) and $DyCl_3 \cdot 6H_2O$ (0.0754 g, 0.2 mmol) in methanol (20 mL) was stirred with triethylamine (0.08 mL, 0.6 mmol) at ambient temperature. After 12 h, this yellow solution was transferred to 25 mL glassware, sealed and kept in a vacuum drying oven at 100 °C. Pale-yellow block-shaped crystals, suitable for X-ray diffraction analysis, were formed after one day as a single-phase product. Yield: 27 mg (31%, based on Dy). Elemental analysis calcd (%) for $C_{13}H_{18}DyN_7O_5Cl_2$: C, 26.66, H, 3.10, N, 16.74: found C, 24.98, H, 3.17, N, 16.02. IR (KBr, cm^{-1}): 3426-2591(br), 1673(s), 1619(m), 1553(vs), 1490(w), 1456(w), 1413(m), 1379(s), 1316(w), 1218(m), 1190(m), 1169(m), 1120(w), 1057(m), 1023(m), 890(w), 764(w), 7751(w), 701(w), 575(m), 526(w), 476(w). Thermal analysis revealed that the weight loss below 110 °C was 12.8%, in agreement with the release of three manthanol molecules (calcd. 12.1%).

Dimer 2-Y:

For $Y_2Cl_2(ppch)(H_2pc)_2 \cdot 4MeOH$ (**2-Y**): The pale-yellow crystals were prepared using the same procedure as for **2** except that $YCl_3 \cdot 6H_2O$ (0.0607 g, 0.2 mmol) was

used as the starting material. Yield: 32 mg (35%, based on Y). Elemental analysis calcd (%) for $C_{13}H_{18}YN_7O_5Cl_2$: C, 30.49, H, 3.54, N, 19.14: found C, 29.56, H, 3.63, N, 18.02. IR (KBr, cm^{-1}): 3492-2659(br), 1667(s), 1611(s), 1552(vs), 1488(w), 1456(w), 1431(m), 1381(s), 1316(w), 1291(w), 1214(m), 1195(m), 1159(m), 1131(w), 1067(m), 1011(m), 876(w), 775(w), 742(w), 703(w), 571(w), 525(w), 468(m), 449(w). Thermal analysis revealed that the weight loss below 115 °C was 15.1%, in agreement with the release of four manthanol molecules (calcd. 14.6%).

Dimer 2-$Dy_{0.50}Y_{0.50}$:

The site-substituted **2-$Dy_{0.50}Y_{0.50}$** sample was synthesized in accordance with the synthesis of pure **2**, with an accurately measured 1:1 molar ratio of dysprosium(III) and yttrium(III) chloride starting materials. IR (KBr, cm-1): 3422-2689(br), 1669(s), 1616(s), 1549(vs), 1493(w), 1462(w), 1416(m), 1386(s), 1324(m), 1278(w), 1217(m), 1199(m), 1170(s), 1132(w), 1063(m), 1001(m), 889(m), 770(w), 739(m), 709(w), 579(m), 525(m), 479(s), 429(w).

Dimer 2-$Dy_{0.10}Y_{0.90}$:

The site-substituted **2-$Dy_{0.10}Y_{0.90}$** sample was synthesized in accordance with the synthesis of pure **2**, with an accurately measured 1:9 molar ratio of dysprosium(III) and yttrium(III) chloride starting materials. IR (KBr, cm-1): 3435-2699(br), 1681(s), 1627(s), 1605(vs), 1535(vs), 1466(w), 1413(m), 1389(s), 1313(w), 1205(m), 1176(m), 1052(m), 1021(m), 906(m), 875(m), 768(w), 739(w), 661(w), 616(w), 576(m), 523(m), 486(w), 445(m), 426(w).

Analytical Procedures

General methods: Elemental analyses for C, H, and N were carried out on a PE 240C elemental analyzer. The infrared spectra were recored as KBr pellets on a Bruker Tensor 27 spectrometer in the range of 400-4000 cm^{-1}. Thermal analyses were performed on a METTLER TOLEDO TGA/DSC 1 instrument in the range of 30-800 °C with Al_2O_3 pan at a heating rate of 5 ºC/min. Powder X-ray diffraction data were collected using a Bruker D8 ADVANCE PXRD equipped with a CuKα X-ray source over the 2θ range of 5 to 50° at room temperature. The UV-vis and luminescence

spectra were recorded on Perkin Elmer Lambda 950 UV/Vis/NIR Spectrometer and Perkin Elmer LS55 fluorescence spectrometer at room temperature, respectively. Atomic composition and scanning electronic micrographs of bulk samples were estimated by the energy-dispersive X-ray spectroscopy (EDX) measurements (SHI-MADZU SSX-550). The magnetic susceptibility data were obtained on a Quantum Design MPMS3 SQUID system. The direct current measurements were obtained with an external magnetic field of 1.0 kOe in the temperature range 1.8-300 K, and the alternating-current measurements were executed in a 3.0 Oe *ac* oscillating field at different frequencies from 1 to 1000 Hz. The diamagnetic contribution of the sample itself was estimated from Pascal's constant.[S1]

*Angular dependent magnetic measurements of **1**:* Angular-dependent magnetic measurements were carried out on a MPMS3 horizontal rotator. A large single crystal (m = 0.26 mg) of **1** was a yellow rhomboid with dimensions of 0.35 mm × 0.30 mm × 0.22 mm. The single crystal was first indexed in an Agilent Xcalibur Eos Gemini CCD diffractometer. Then this crystal was mounted on the Standard sample platform. Subsequently, three rotations were performed under 3.0 kOe at 5.0 K. The diamagnetic background of the sample rotator and the beryllium copper slice was corrected from the signal of the magnetization.

*Themperature variable specific heat capacity (C_p-T curve) of **1**:* Temperature-dependent heat capacity measurements were recorded on a Quantum Design PPMS Model 6000 PPMS with a heat capacity measurement option (Model 6500). A powdered sample of **1** used in this study was 102 mg, the highest applied field was 3.0 T, and the temperature regime was 1.9-13.0 K.

*Magneto-photoluminescence measurements of **1**:* Multimode optical fibers were used to transmit both the excitation and emission light beams. The PL was excited by a solid-state laser with the wavelength of 402 nm and recorded by a spectrometer composed of a monochromator (SP500i, Andor) and an electron-multiplied charge coupled device (EMCCD, Newton 970P, Andor). The samples were placed into a liquid helium cryostat at the center of a pulsed magnet with the designed peak field of

50 T and pulse duration of 100 ms. In this situation, the EMCCD was exposed every millisecond synchronous to the time period of the magnetic field pulse.

Crystal structure determination and refinement: Single crystal of dimension 0.15 × 0.12 × 0.11 mm^3 for dimer compound **2** was selected for indexing and intensity data collection on a Bruker P4 CCD diffractometer equipped with graphite-monochromated Mo Kα radiation (λ = 0.71073 Å) at room temperature. Single crystals of dimensions 0.12 × 0.12 × 0.11 mm^3 for dimer compound **2-Y**, 0.16 × 0.16 × 0.12 mm^3 for compound **1**, 0.14 × 0.14 × 0.12 mm^3 for compound **1-Y** were selected for indexing and intensity data collection on an Agilent Xcalibur Eos Gemini CCD plate diffractometer using graphite-monochromated Cu Kα radiation (λ = 1.54184 Å) at room temperature. The numbers of collected and observed independent [$I > 2\sigma(I)$] reflections are 10636 and 3645 (R_{int} = 0.0268) for dimer **2**, 6496 and 3669 (R_{int} = 0.0355) for **2-Y**, 11224 and 3054 (R_{int} = 0.0507) for **1**, 10499 and 3047 (R_{int} = 0.0228) for **1-Y**. The data were integrated with the Siemens SAINT program.[S2] Absorption corrections were utilized.[S3] All the structures were solved by direct methods and refined on F^2 by full-matrix least squares using the SHELXTL-2014 program suite.[S4] Anisotropic thermal parameters were used for refinement of all nonhydrogen atoms. All hydrogen atom positions were computed geometrically and were riding on their respective atoms. CCDC 2222488 (**2**), CCDC 2222489 (**2-Y**), CCDC 2222490 (**1**) and CCDC 2222491 (**1-Y**) contain the supplementary crystallographic data for this paper. These data can be obtained free of charge from the Cambridge Crystallographic Data Centre via www.ccdc.cam.ac.uk/data_request/cif.

S2 Structure information

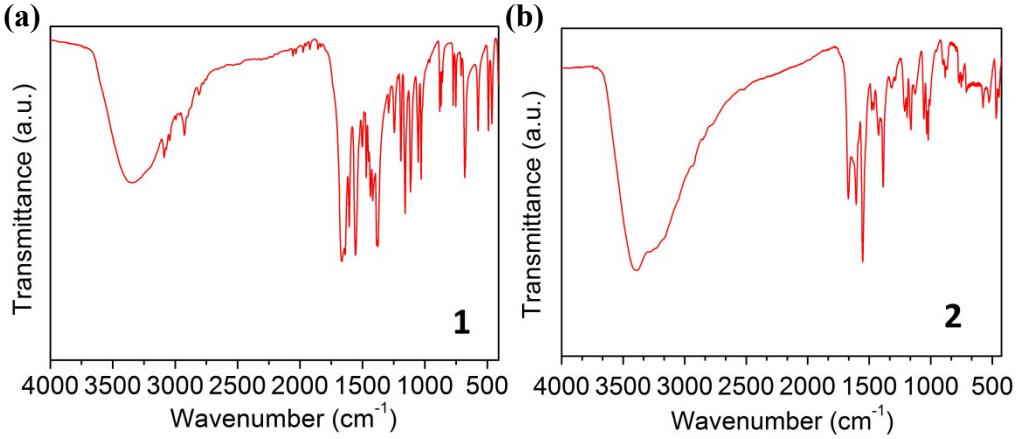

Figure S1. Infrared spectra of compounds **1** (a) and **2** (b).

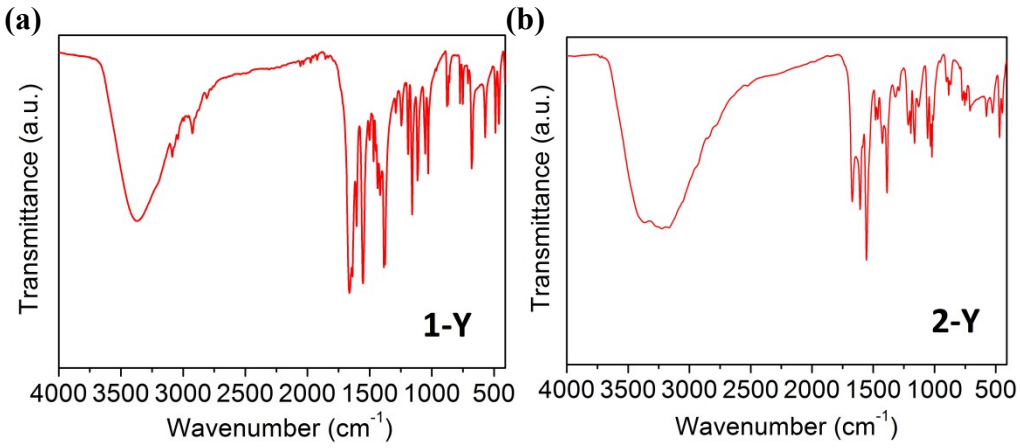

Figure S2. Infrared spectra of compounds **1-Y** (a) and **2-Y** (b).

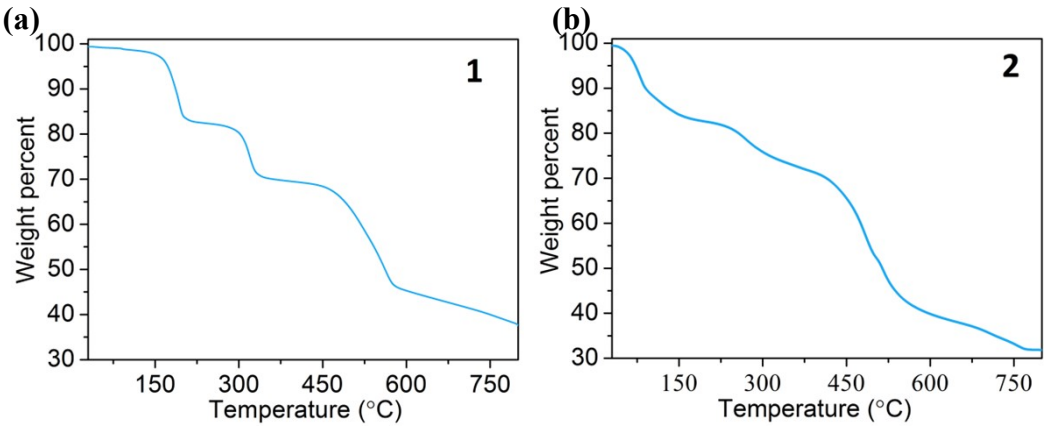

Figure S3. Thermal analysis of compounds **1** (a) and **2** (b).

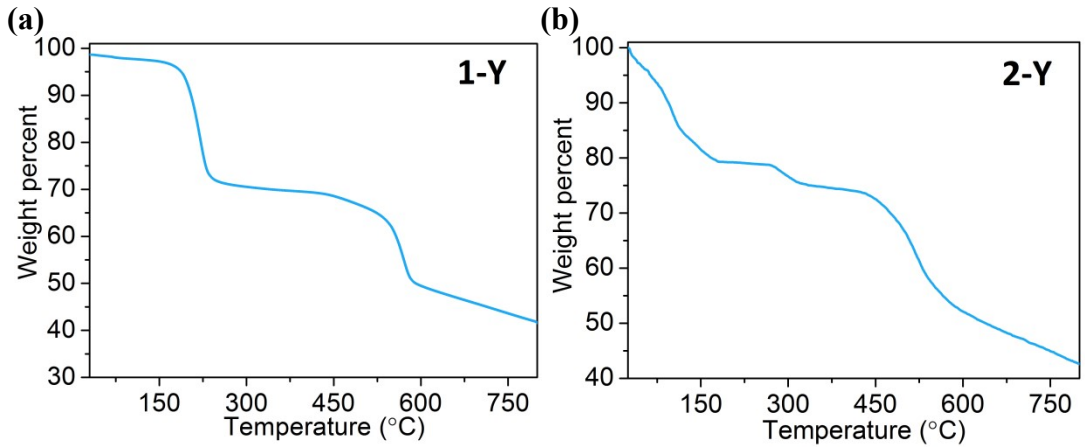

Figure S4. Thermal analysis of compounds **1-Y** (a) and **2-Y** (b).

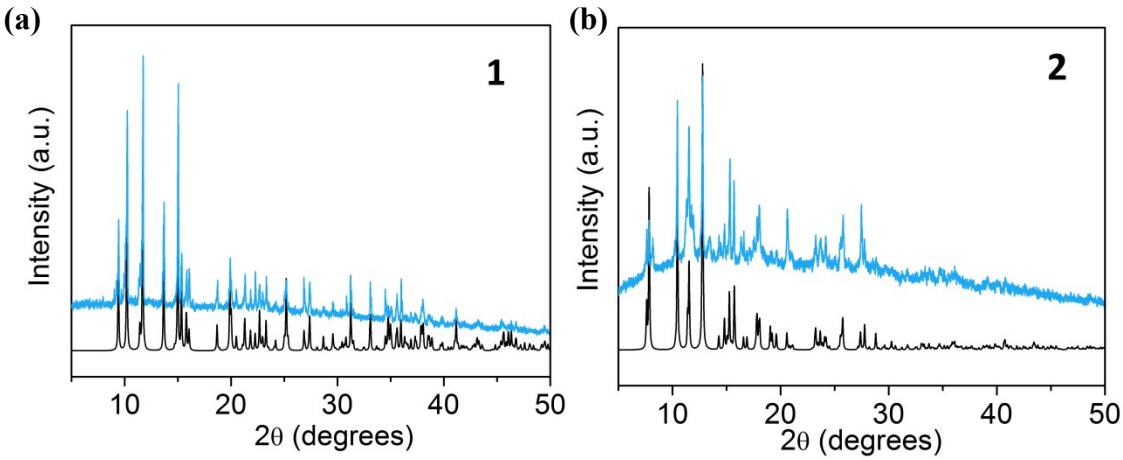

Figure S5. The powder XRD patterns of compounds **1** (a) and **2** (b).

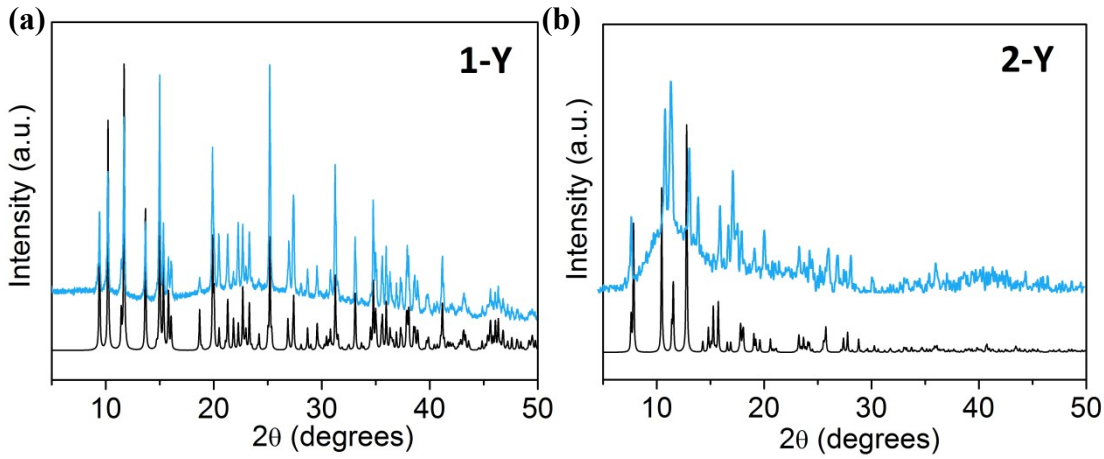

Figure S6. The powder XRD patterns of compounds **1-Y** (a) and **2-Y** (b).

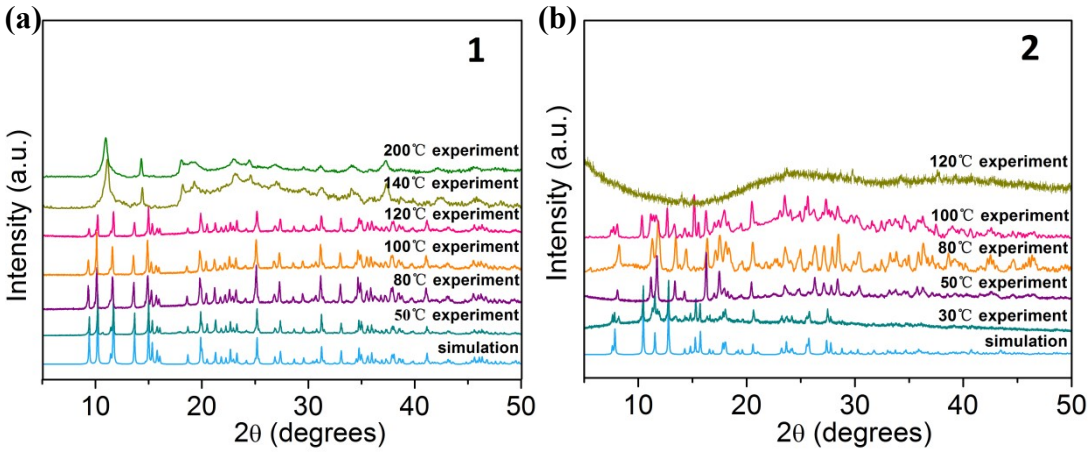

Figure S7. Powder X-ray diffraction data for compounds **1** (left) and **2** (right) under vacuum at different temperatures.

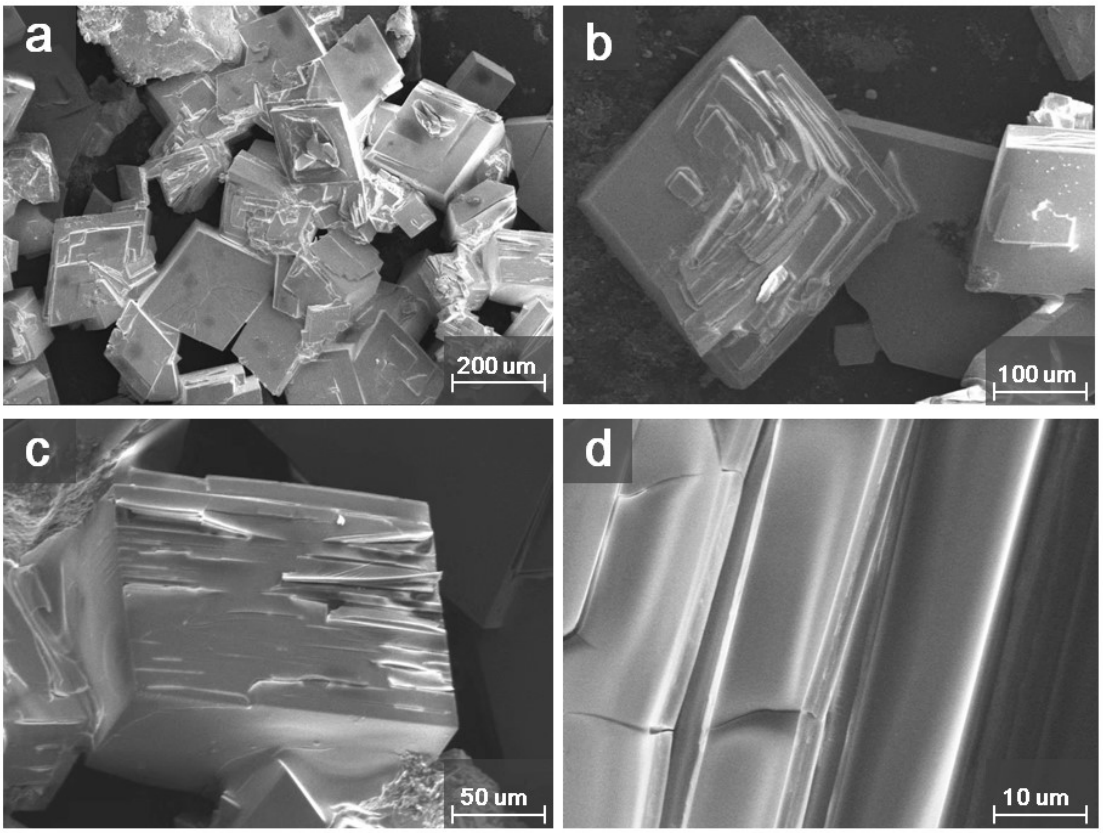

Figure S8. Scanning electron micrograph of bulk-type **1**.

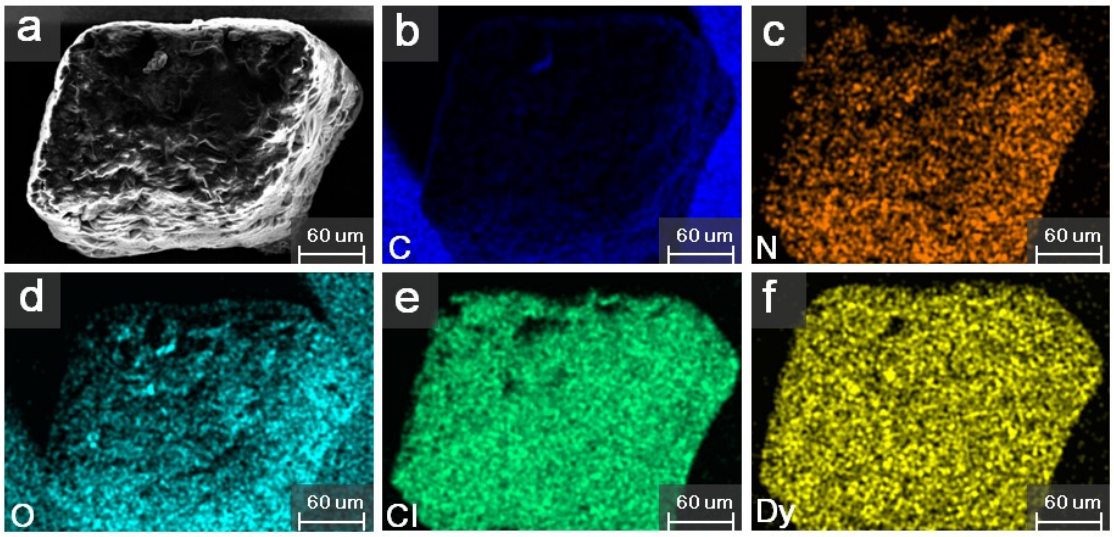

Figure S9. Elemental mapping of compound **1**.

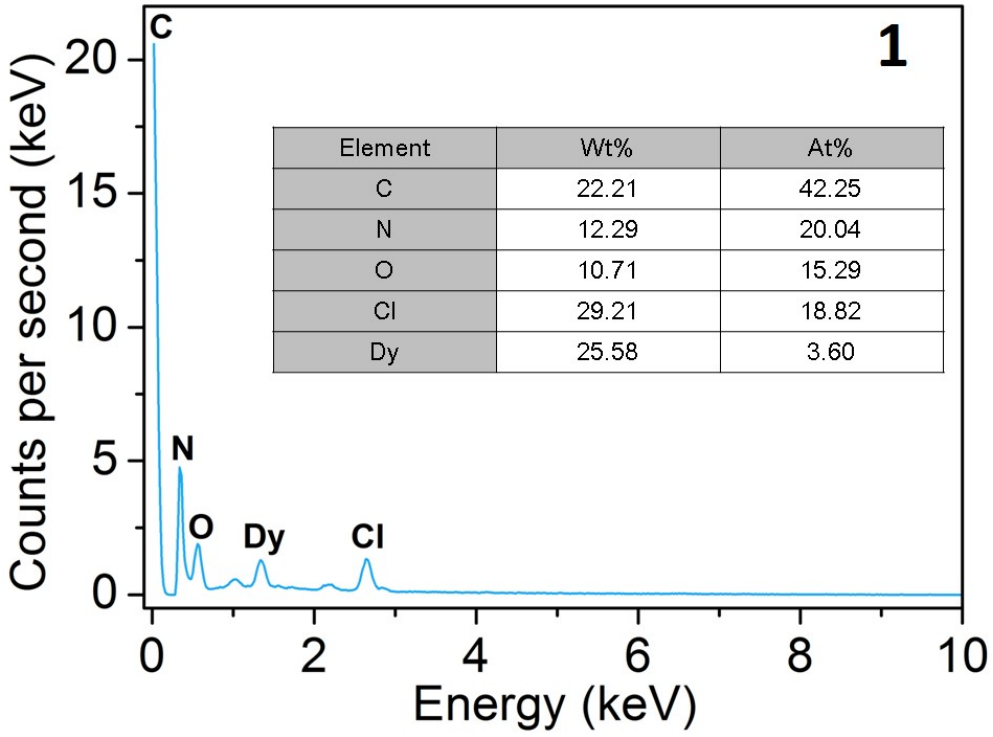

Element	Wt%	At%
C	22.21	42.25
N	12.29	20.04
O	10.71	15.29
Cl	29.21	18.82
Dy	25.58	3.60

Figure S10. EDX analysis of compound **1**.

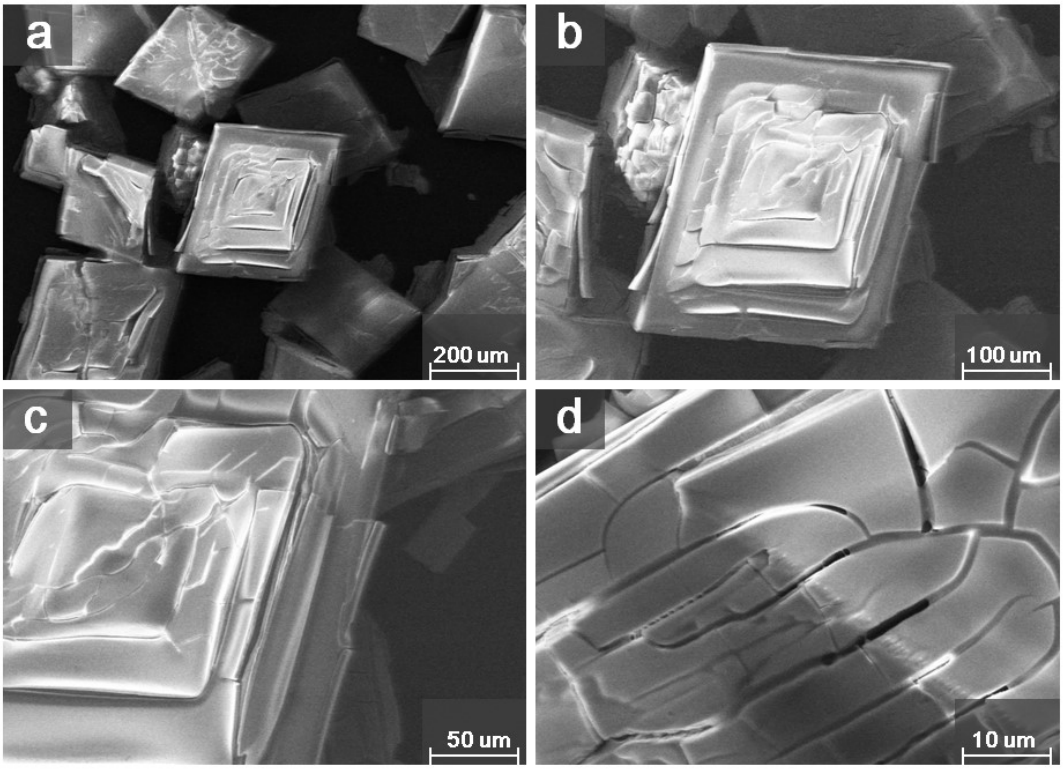

Figure S11. Scanning electron micrograph of bulk-type **1-$Dy_{0.50}Y_{0.50}$**.

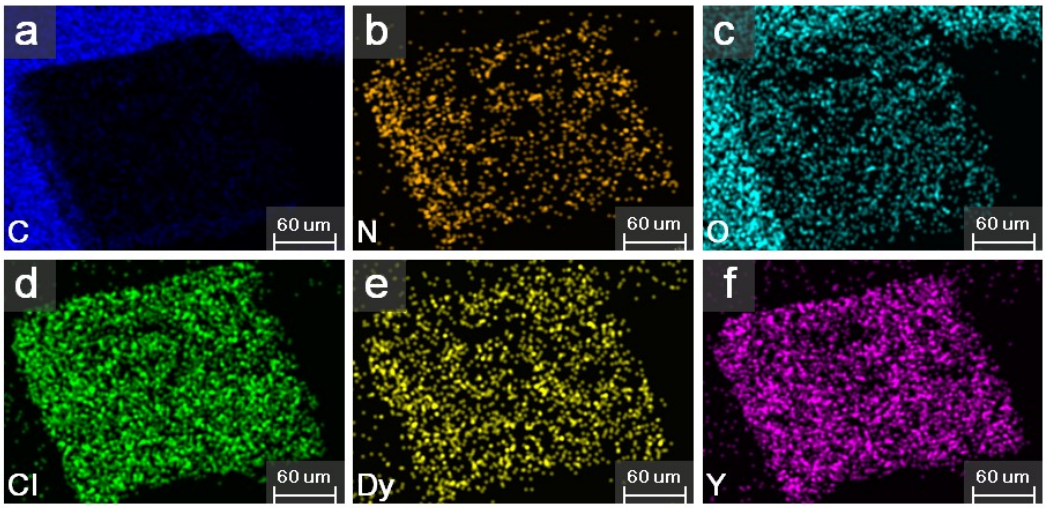

Figure S12. Elemental mapping of compound **1-$Dy_{0.50}Y_{0.50}$**.

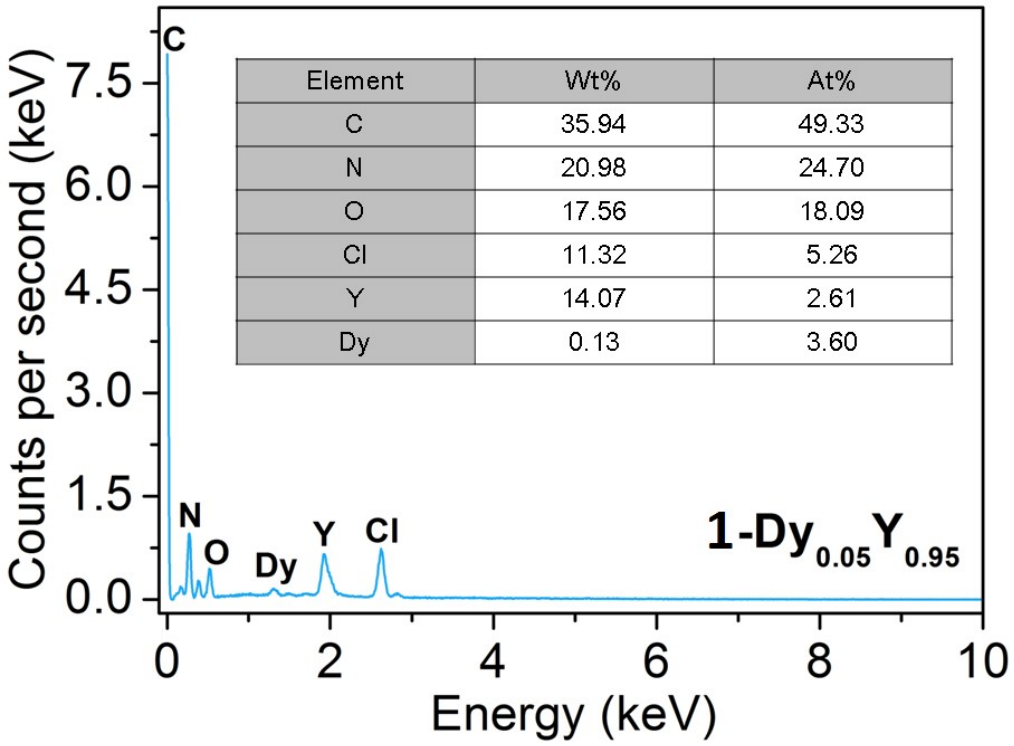

Element	Wt%	At%
C	35.94	49.33
N	20.98	24.70
O	17.56	18.09
Cl	11.32	5.26
Y	14.07	2.61
Dy	0.13	3.60

Figure S13. EDX analysis of compound **1-$Dy_{0.50}Y_{0.50}$**.

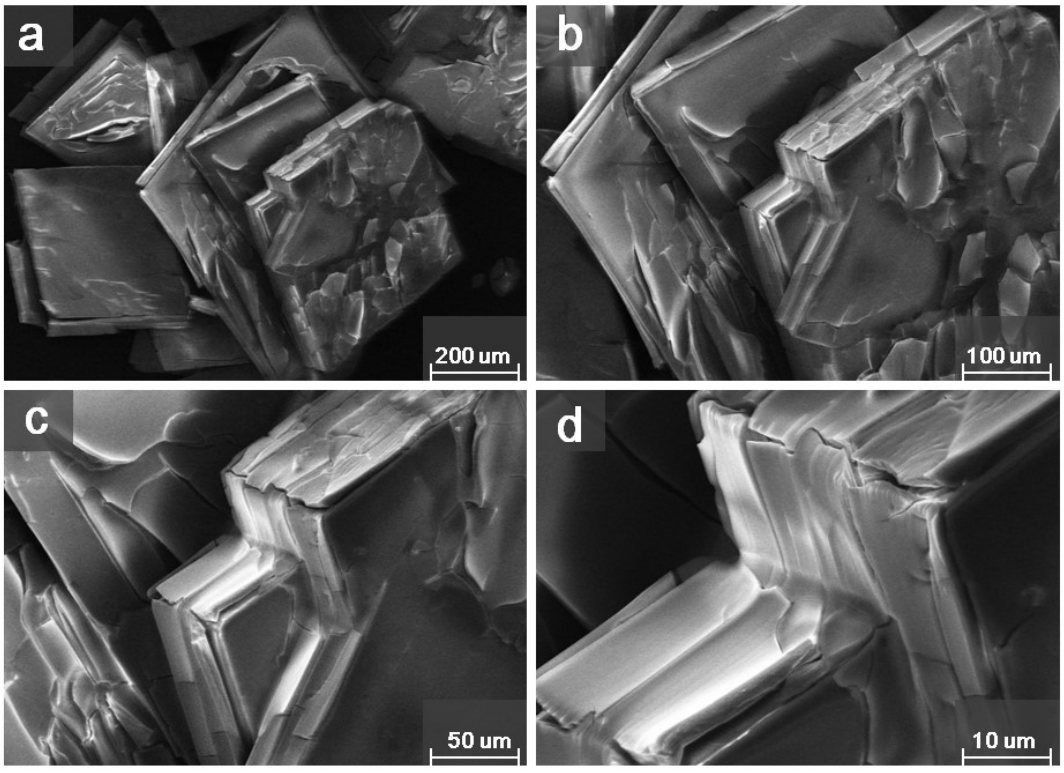

Figure S14. Scanning electron micrograph of bulk-type **1-$Dy_{0.10}Y_{0.90}$**.

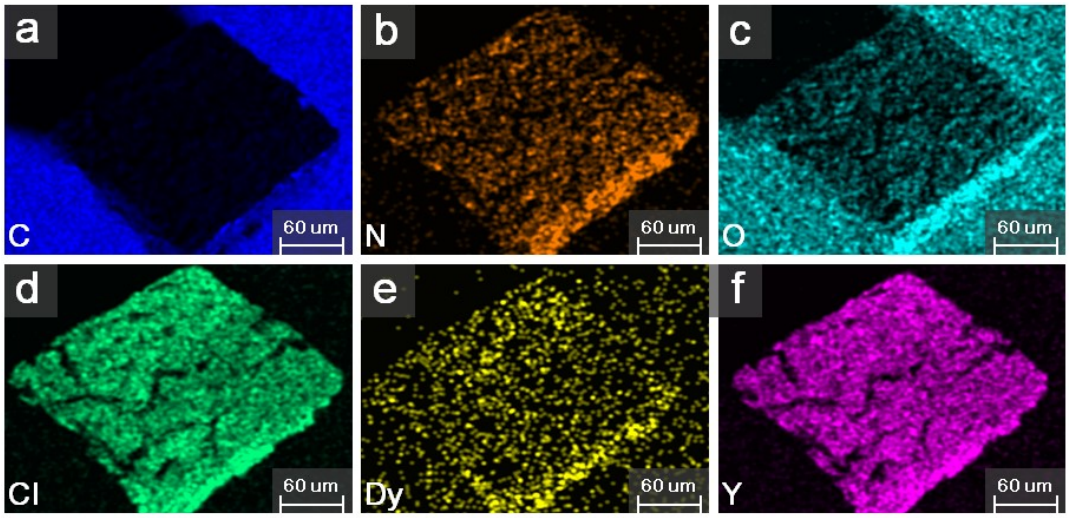

Figure S15. Elemental mapping of compound **1-$Dy_{0.10}Y_{0.90}$**.

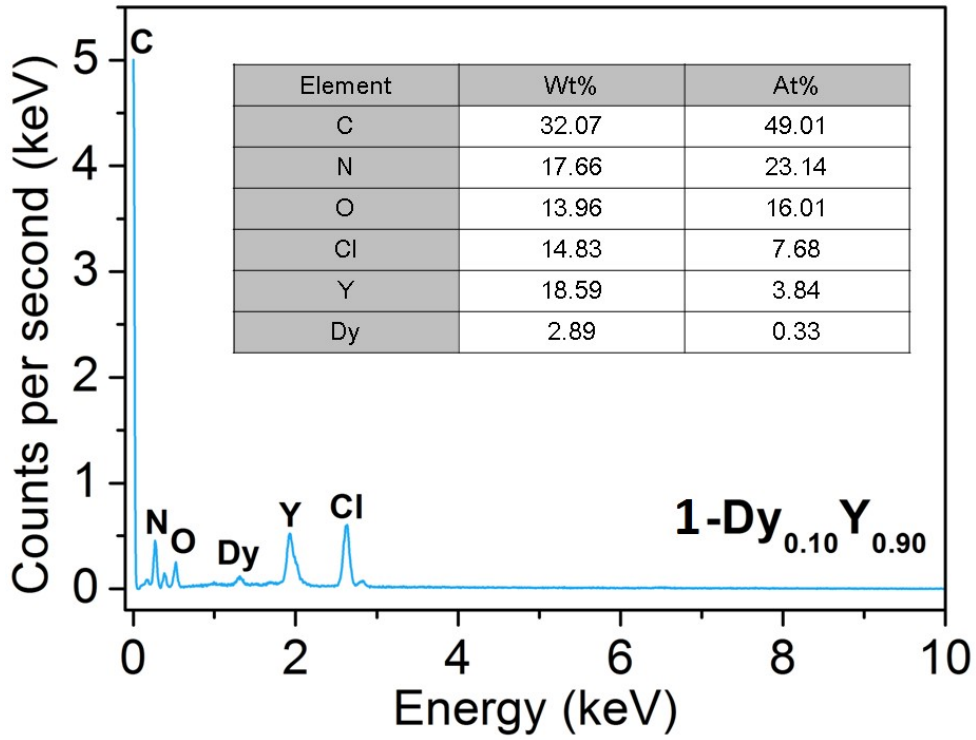

Element	Wt%	At%
C	32.07	49.01
N	17.66	23.14
O	13.96	16.01
Cl	14.83	7.68
Y	18.59	3.84
Dy	2.89	0.33

Figure S16. EDX analysis of compound **1-$Dy_{0.10}Y_{0.90}$**.

Table S1. Summary of structural data of compounds **1**, **1-Y**, **2** and **2-Y**.

	1	**1-Y**	**2**	**2-Y**
CCDC number	2222490	2222491	2222488	2222489
Empirical formula	$C_{11}H_{17}DyN_5O_3Cl_2$	$C_{11}H_{17}YN_5O_3Cl_2$	$C_{13}H_{18}DyN_7O_5Cl_2$	$C_{13}H_{18}YN_7O_5Cl_2$
Formula weight	500.69	427.10	585.74	515.18
Crystal size (mm^3)	0.16× 0.16× 0.12	0.14× 0.14× 0.12	0.15× 0.12× 0.11	0.12× 0.12× 0.11
Temperature (K)	293(2)	293(2)	293(2)	293(2)
Crystal system	Monoclinic	Monoclinic	Triclinic	Triclinic
Space group	$P2_1/n$ #14	$P2_1/n$ #14	P-1 #2	P-1 #2
a (Å)	9.3158(4)	9.3046(4)	7.871(3)	7.8517(4)
b (Å)	15.4758(6)	15.4723(4)	11.468(5)	11.4428(6)
c (Å)	12.6904(6)	12.6691(6)	11.794(5)	11.7839(6)
α (°)	90	90	93.420(4)	93.243(4)
β (°)	111.421(5)	111.294(5)	98.291(5)	98.344(4)
γ (°)	90	90	99.303(6)	99.482(4)
Volume ($Å^3$)	1703.19(14)	1699.36(13)	1035.8(7)	1029.68(9)
Z	4	4	2	2
ρ_{calcd} (g/cm^3)	1.953	1.669	1.878	1.662
2θ (deg)	4.7 – 67.2	4.712 – 67.237	2.621 – 25.018	3.930 – 67.248
F(000)	968	860	570	522
Reflns collected	11224	10499	10636	6496
Unique reflns	3054	3047	3645	3669
R_{int}	0.0507	0.0228	0.0268	0.0355
GOF	1.036	1.074	1.108	1.063
$R1$[a]	0.0326	0.0248	0.0240	0.0384
w$R2$[b]	0.0815	0.0657	0.0529	0.1032

Table S2. Selected bond lengths (Å) and angles (º) for compound **1**.

1					
Dy1–O2a	2.319(3)	O3-Dy1-O4	71.00(14)	C4-N1-Dy1	115.0(3)
Dy1–O3	2.331(3)	O2a-Dy1-N5	65.44(10)	C2-N2-C3	116.4(4)
Dy1–O4	2.386(4)	O3-Dy1-N5	75.20(12)	C2-N2-Dy1c	126.3(3)
Dy1–N5	2.425(3)	O4-Dy1-N5	126.56(13)	C3-N2-Dy1c	117.3(3)
Dy1–Cl1	2.6663(15)	O2a-Dy1-Cl2	156.15(8)	C6-N3-C7	120.9(5)
Dy1–Cl2	2.6498(12)	O3-Dy1-Cl2	93.99(10)	C6-N3-C8	121.9(5)
Dy1–N1	2.740(4)	O4-Dy1-Cl2	84.56(10)	C7-N3-C8	117.2(5)
Dy1–N2b	2.685(4)	N5-Dy1-Cl2	138.41(8)	C9-N4-C10	120.6(5)
N1-C1	1.331(6)	O2a-Dy1-Cl1	89.66(9)	C9-N4-C11	121.7(6)
N1-C4	1.339(6)	O3-Dy1-Cl1	147.97(10)	C10-N4-C11	117.7(5)
N2-C2	1.328(6)	O4-Dy1-Cl1	140.14(10)	C5-N5-N5a	111.4(4)
N2-C3	1.330(6)	N5-Dy1-Cl1	77.02(9)	C5-N5-Dy1	130.2(3)
N3-C6	1.303(6)	Cl2-Dy1-Cl1	96.28(5)	N5a-N5-Dy1	118.4(3)
N3-C7	1.457(7)	O2a-Dy1-N2b	76.81(11)	C5-O2-Dy1a	119.2(3)
N3-C8	1.459(7)	O3-Dy1-N2b	139.80(12)	C6-O3-Dy1	136.7(3)
N4-C9	1.297(7)	O4-Dy1-N2b	68.81(13)	C9-O4-Dy1	134.1(4)
N4-C10	1.455(8)	N5-Dy1-N2b	130.48(11)	N1-C1-C2	122.3(4)
N4-C11	1.459(7)	Cl2-Dy1-N2b	83.15(8)	N2-C2-C1	121.7(4)
N5-C5	1.294(5)	Cl1-Dy1-N2b	71.73(9)	N2-C3-C4	121.8(4)
N5-N5a	1.393(7)	O2a-Dy1-N1	127.23(11)	N1-C4-C3	122.3(4)
O2-C5	1.293(5)	O3-Dy1-N1	74.42(12)	N1-C4-C5	118.2(4)
O3-C6	1.250(6)	O4-Dy1-N1	139.08(13)	C3-C4-C5	119.5(4)
O4-C9	1.236(7)	N5-Dy1-N1	61.79(11)	O2-C5-N5	125.5(4)
C1-C2	1.392(7)	Cl2-Dy1-N1	76.62(8)	O2-C5-C4	119.6(4)
C3-C4	1.386(6)	Cl1-Dy1-N1	78.60(8)	N5-C5-C4	114.9(4)
C4-C5	1.489(6)	N2b-Dy1-N1	141.78(11)	O3-C6-N3	124.5(5)
O2a -Dy1-O3	93.06(12)	C1-N1-C4	115.4(4)	O4-C9-N4	125.9(6)
O2a-Dy1-O4	76.27(12)	C1-N1-Dy1	129.6(3)		

Symmetry codes: (a) -x+1, -y, -z; (b) -x+3/2, y+1/2, -z+1/2; (c) -x+3/2, y-1/2, -z+1/2.

Table S3. Selected bond lengths (Å) and angles (º) for compound **2**.

2					
Dy1-O1	2.373(8)	Cl1-Dy1-N1	78.71(19)	C3-N2-N1	116.3(8)
Dy1-O2	2.390(7)	Cl1-Dy1-N5a	139.66(19)	C4-N3-C5	116.4(10)
Dy1-O3	2.379(7)	Cl1-Dy1-N7a	78.36(18)	C7-N4-C6	117.9(11)
Dy1-O4	2.330(6)	O1-Dy1-O2	151.0(3)	C8-N5-N5a	111.4(9)
Dy1-N1	2.579(8)	O1-Dy1-O3	72.4(3)	C8-N5-Dy1a	130.6(6)
Dy1-Cl1	2.642(2)	O1-Dy1-O4	97.2(2)	N5a-N5-Dy1a	118.0(7)
Dy1-N5a	2.389(7)	O1-Dy1-N1	137.1(3)	C10-N6-C11	117.5(9)
Dy1-N7a	2.667(8)	O1-Dy1-N5a	76.8(3)	C12-N7-C9	114.9(8)
C1-O1	1.431(16)	O1-Dy1-N7a	73.1(3)	C12-N7-Dy1a	127.6(6)
C2-O2	1.416(17)	O2-Dy1-O3	136.0(3)	C9-N7-Dy1a	117.0(6)
C3-O3	1.228(11)	O2-Dy1-O4	86.2(2)	O3-C3-N2	124.5(8)
C8-O4	1.291(11)	O2-Dy1-N1	71.5(3)	O3-C3-C4	120.3(8)
C13-O5	1.390(3)	O2-Dy1-N5a	78.4(3)	N2-C3-C4	115.2(8)
C3-N2	1.321(12)	O2-Dy1-N7a	82.2(3)	N3-C4-C7	123.0(9)
C4-N3	1.307(14)	O3-Dy1-O4	77.9(2)	N3-C4-C3	117.9(9)
C5-N3	1.347(17)	O3-Dy1-N1	64.7	C7-C4-C3	119.0(9)
C7-N4	1.324(19)	O3-Dy1-N5a	128.6(2)	N3-C5-C6	121.8(13)
C6-N4	1.345(18)	O3-Dy1-N7a	138.9(2)	N4-C6-C5	120.0(10)
C8-N5	1.274(12)	O4-Dy1-N1	74.0(2)	N4-C7-C4	120.9(12)
N5-N5a	1.415(10)	O4-Dy1-N5a	66.3(2)	N5-C8-O4	126.9(8)
C11-N6	1.326(14)	O4-Dy1-N7a	128.2(2)	N5-C8-C9	115.3(8)
C10-N6	1.323(14)	N1-Dy1-N5a	131.1(3)	O4-C8-C9	117.9(7)
C12-N7	1.343(12)	N1-Dy1-N7a	144.8(2)	N7-C9-C10	122.1(8)
N1-N2	1.419(11)	N5a-Dy1-N7a	61.9(3)	N7-C9-C8	114.9(8)
C9-N7	1.354(12)	C1-O1-Dy1	130.3(8)	C10-C9-C8	122.9(8)
Cl1-Dy1-O1	99.3(2)	C2-O2-Dy1	133.2(8)	N6-C10-C9	122.3(9)
Cl1-Dy1-O2	90.08(18)	C3-O3-Dy1	122.2(5)	N6-C11-C12	120.6(9)
Cl1-Dy1-O3	85.85(17)	C8-O4-Dy1	117.4(5)	N7-C12-C11	122.6(9)
Cl1-Dy1-O4	152.17(15)	N2-N1-Dy1	111.9(5)		

Symmetry codes: (a) -x+1, -y+2, -z+1.

Table S4. Hydrogen bonds for compound **1**.

1				
D–H···A	**d(D–H) (Å)**	**d(H···A) (Å)**	**d(D···A) (Å)**	**<(DHA) (º)**
C1-H1···Cl2	0.9300	2.7200	3.357(5)	126.00
C2-H2···O2	0.9300	2.6000	3.185(6)	121.00
C3-H3 ···O2	0.9300	2.4900	2.812(6)	101.00
C3-H3···Cl2	0.9300	2.5600	3.316(5)	139.00
C7-H7a···O3	0.9600	2.3600	2.769(8)	105.00
C7-H7c···Cl1	0.9600	2.7800	3.597(7)	144.00
C9-H9···O2	0.9300	2.4800	3.023(7)	117.00
C10-H10a···O4	0.9600	2.3700	2.774(8)	105.00
C11-H11c···Cl1	0.9600	2.7800	3.607(7)	144.00

Symmetry codes: (a) 3/2-x, -1/2+y, 1/2-z; (c) 1-x, -y, -z.

Table S5. Hydrogen bonds for compound **2**.

2				
D–H···A	**d(D–H) (Å)**	**d(H···A) (Å)**	**d(D···A) (Å)**	**<(DHA) (º)**
N1-H1b···N4	0.9000	2.5500	3.420(17)	164.00
N2-H2···N3	0.8600	2.3500	2.693(13)	104.00
N2-H2···N6	0.8600	2.0700	2.906(12)	165.00
O5-H5···N1	0.8200	2.5600	2.943(17)	110.00
O5-H5···Cl2	0.8200	2.8300	3.180(16)	108.00
C1-H1c···O3	0.9600	2.4300	3.040(17)	121.00
Cl2-H12···Cl1	0.9300	2.6900	3.338(10)	128.00

Symmetry codes: (b) -1+x, y, -1+z; (c) -1+x, y, z.

Table S6. Dy^{III} geometry analysis of **1** and **2** by SHAPE 2.1 software.

1 (CN = 8)							
JBTPR	BTPR	JSD	TDD	SAPR	JGBF		CU
3.598	2.774	2.982	1.690	3.890	11.829		13.398
TT	HBPY	ETBPY	JETBPY	HPY	OP		
14.091	15.201	25.415	27.630	25.098	31.526		
2 (CN = 8)							
JBTPR	BTPR	JSD	TDD	SAPR	JGBF		CU
3.266	2.657	2.979	1.890	4.393	11.076		13.282
TT	HBPY	ETBPY	JETBPY	HPY	OP		
13.815	14.471	23.567	25.716	24.823	31.563		
Lable	Shape	Lable	Shape	Lable	Shape	Lable	Shape
JBTPR	Biaugmented trigonal prism J50 (C_{2v})	BTPR	Biaugmented trigonal prism (C_{2v})	JSD	Snub diphenoid J84 (D_{2d})	TDD	Triangular dodecahedron (D_{2d})
SAPR	Square antiprism (D_{4d})	JGBF	Johnson gyrobifastigium J26 (D_{2d})	CU	Cube (O_h)	TT	Triakis tetrahedron (T_d)
HBPY	Hexagonal bipyramid (D_{6h})	ETBPY	Elongated trigonal bipyramid (D_{3h})	JETBPY	Johnson elongated triangular bipyramid J14 (D_{3h})	HPY	Heptagonal pyramid (C_{7v})
OP	Octagon						

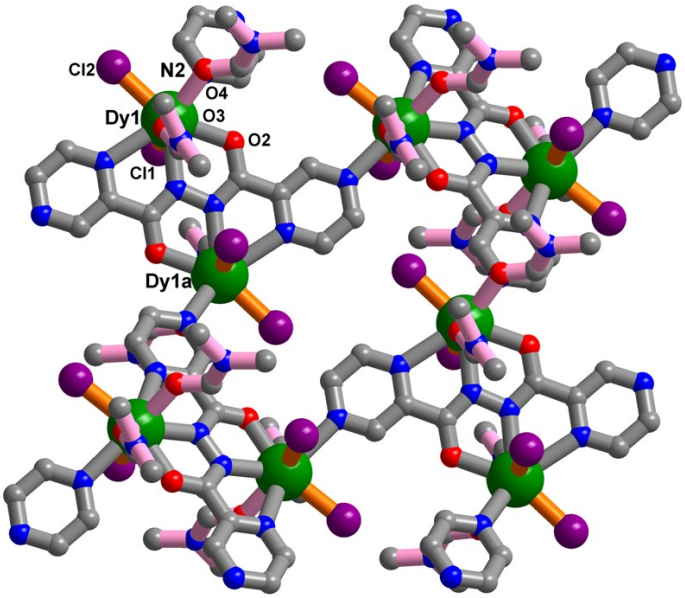

Figure S17. The structure of **1**. All hydrogen atoms are omitted for clarity.

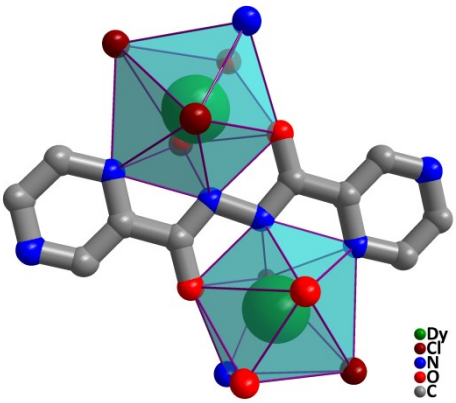

Figure S18. Depiction of coordination polyhedra around the Dy atoms in **1**. Noncoordinating atoms of the ancillary ligands and hydrogen atoms are omitted.

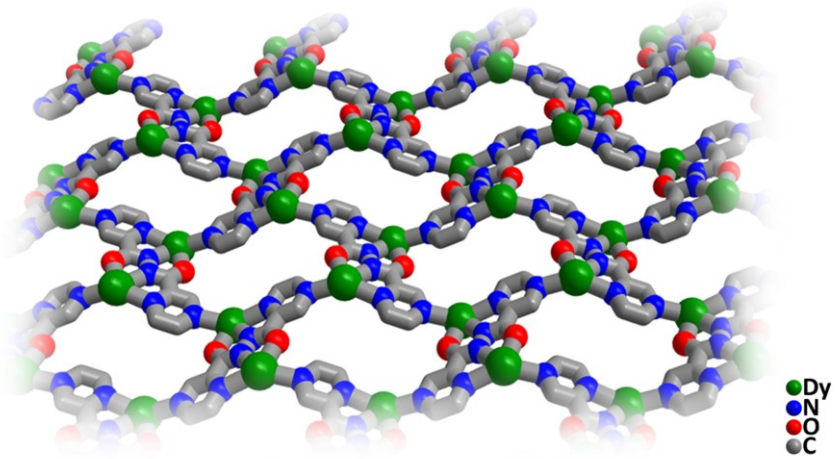

Figure S19. Topological arrangement of the Dy(III) ions in the single layer of **1**. The coordinating chloride anions and DMF molecules are omitted.

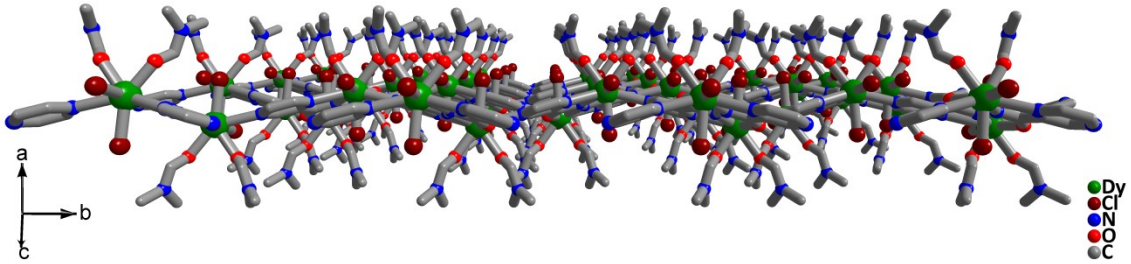

Figure S20. The layer structure of **1** shown along the crystallographic *c*-axis. All hydrogen atoms are omitted for clarity.

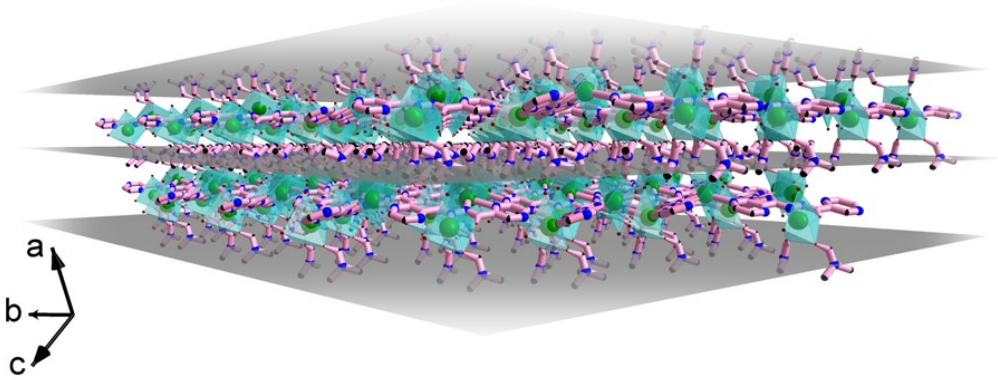

Figure S21. Architecture of the layered **1**. The *bc* planes are highlighted in gray to better illustrate the layered structure

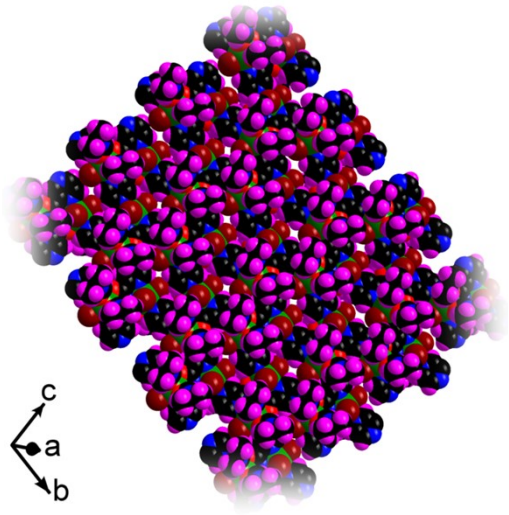

Figure S22. Space-filling representation of compound **1**. Color code: dysprosium, green; chloride, dark red; oxygen, red; nitrogen, blue; carbon, black; hydrogen, pink.

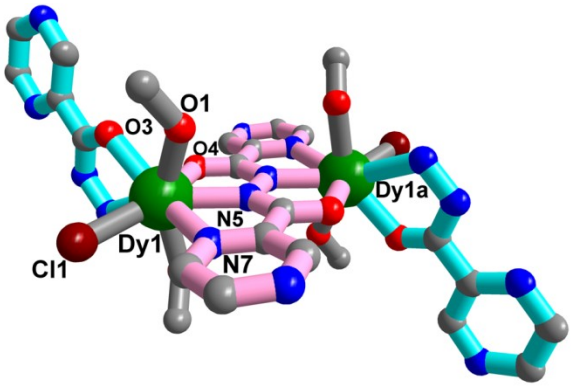

Figure S23. The structure of dimer compound **2**. All hydrogen atoms are omitted for clarity.

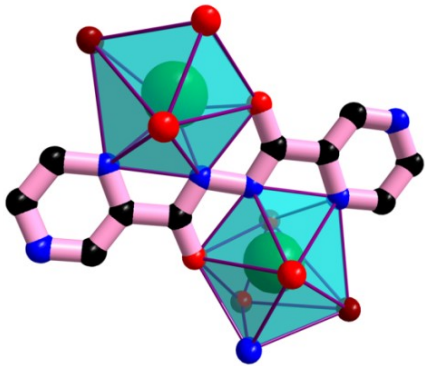

Figure S24. Depiction of coordination polyhedra around the Dy atoms in **2**. Noncoordinating atoms of the ancillary ligands and hydrogen atoms are omitted.

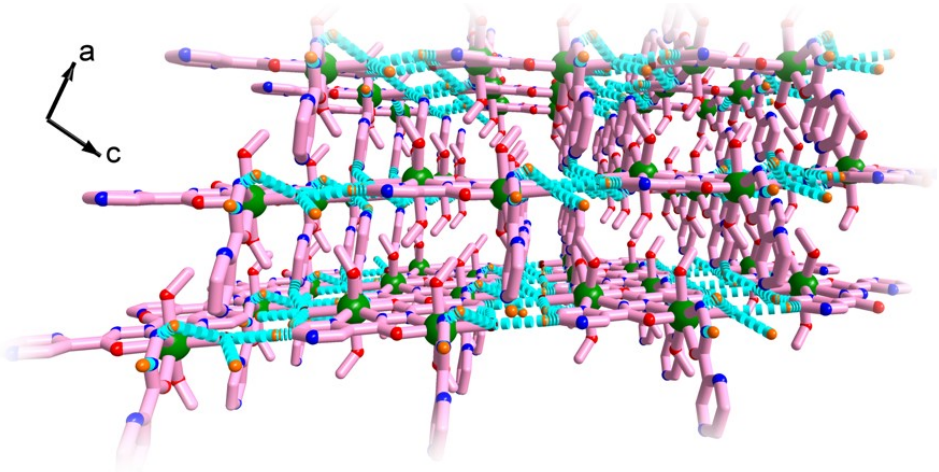

Figure S25. Two-dimensional hydrogen-bonded supramolecular structure in **2** along the *b*-axis. Color scheme: the H-bond in turquoise.

S3 Magnetic properties of 1

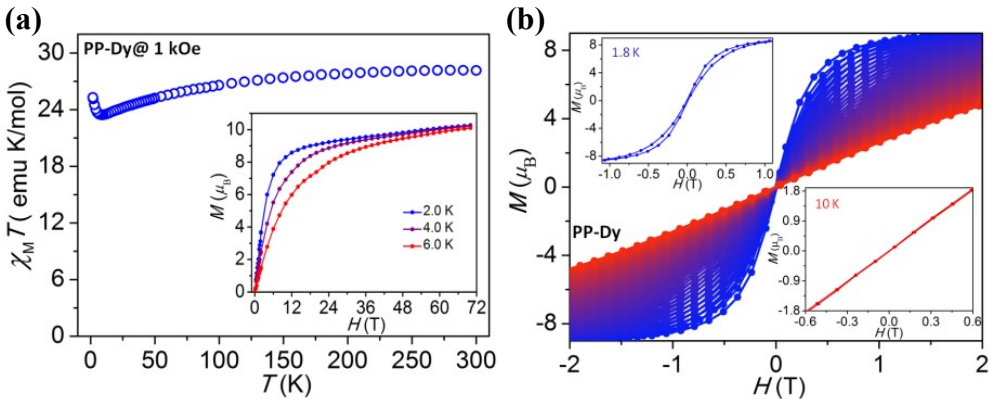

Figure S26. Variable-temperature molar magnetic susceptibility data for **2**, collected under an applied field of 1000 Oe (a). Variable-temperature *M*(*H*) curves collected from 0 to 7 T (b). Magnified view of the plots (b inset).

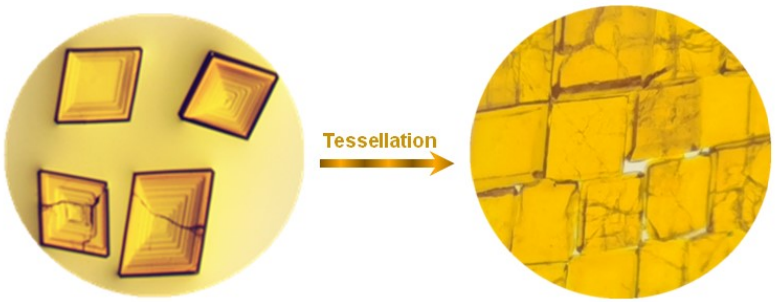

Figure S27. The optical images for crystals of **1** (left). The layer of crystals suitable for anisotropic measurement (right).

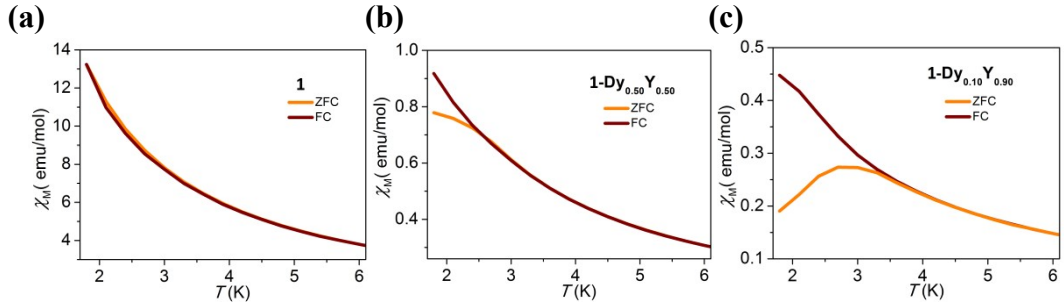

Figure S28. Variable-temperature χ_M magnetic susceptibilities of **1** (a), **1-Dy$_{0.50}$Y$_{0.50}$** (b) and **1-Dy$_{0.10}$Y$_{0.90}$** (c) under field-cooled (FC) and zero-field-cooled (ZFC) conditions with a field of 1.0 kOe.

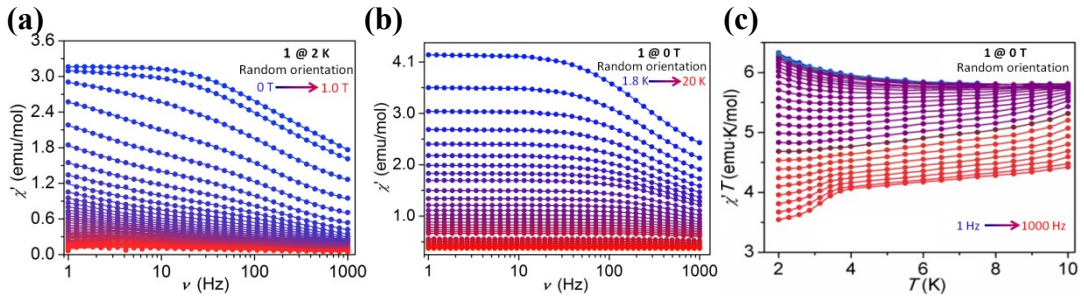

Figure S29. Variable-field χ_M' magnetic susceptibility versus frequency data for **1** (powder sample) on a random orientation, collected at fields ranging from 0 to 1 T at 2.0 K (a). Variable-temperature χ_M' magnetic susceptibility versus frequency data (b) variable-frequency $\chi_M'T$ magnetic susceptibility versus temperature data (c) for compound **1** on a randomly oriented powder sample under zero applied dc field, collected at temperatures ranging from 1.8 to 20.0 K and frequencies from 1.0 to 1000 Hz, respectively.

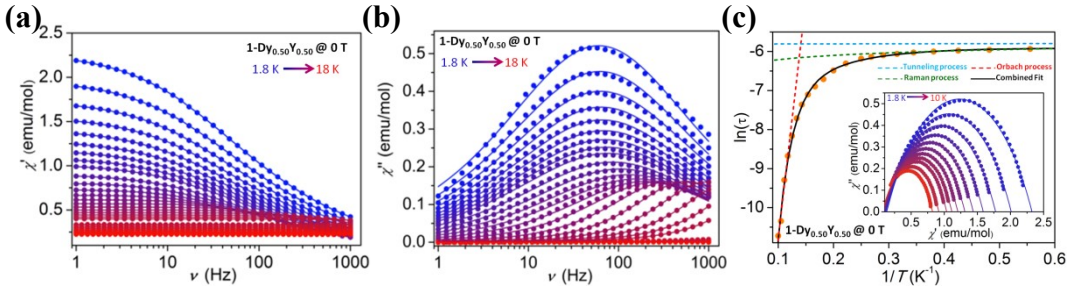

Figure S30. Variable-temperature χ_M' (a) and χ_M'' (b) magnetic susceptibility versus frequency data for compound **1-Dy$_{0.50}$Y$_{0.50}$** (powder sample) on a random orientation, collected at temperatures ranging from 1.8 to 20.0 K under zero applied dc field. Plot of inverse temperature versus the natural log of the magnetization relaxation time (c). Cole-Cole plots (c, inset). The best-fit parameters are obtained by combining Obrach process, Raman process and quantum tunneling of the magnetization ($\tau^{-1} = \tau_0^{-1}\exp(-U_{eff}/k_BT) + CT^n + \tau_{tunnel}^{-1}$) yields the best parameters with U_{eff} = 124.62(5) K, τ_o = 8.06(4) × 10^{-10} s, C = 0.00154(9) s^{-1} $K^{-7.83}$, n = 7.83(2), and τ_{tunnel} = 2.94(6) × 10^{-3} s (Table S8).

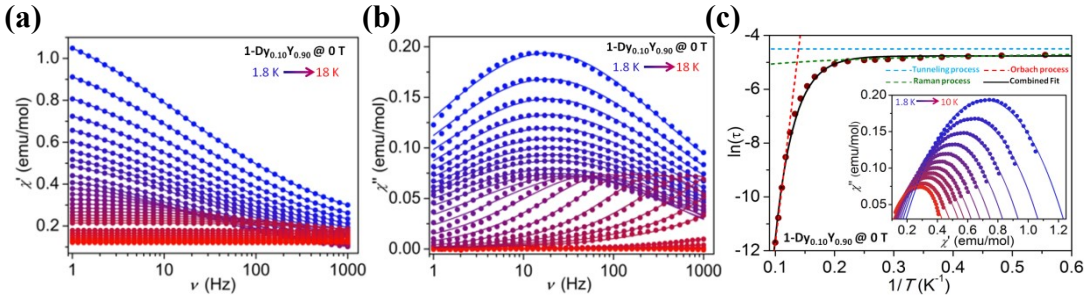

Figure S31. Variable-temperature χ' (a) and χ'' (b) magnetic susceptibility versus frequency data for compound **1-Dy$_{0.10}$Y$_{0.90}$** (powder sample) on a random orientation, collected at temperatures ranging from 1.8 to 20.0 K under zero applied dc field. Plot of inverse temperature versus the natural log of the magnetization relaxation time (c). Cole-Cole plots (c, inset). The best-fit parameters are obtained by combining Obrach process, Raman process and quantum tunneling of the magnetization ($\tau^{-1} = \tau_0^{-1}\exp(-U_{eff}/k_BT) + CT^n + \tau_{tunnel}^{-1}$) yields the best parameters with U_{eff} = 149.18(6) K, τ_o = 8.12(9) × 10^{-10} s, C = 0.00108(2) s^{-1} $K^{-6.94}$, n = 6.94(1), and τ_{tunnel} = 6.02(4) × 10^{-3} s (Table S9).

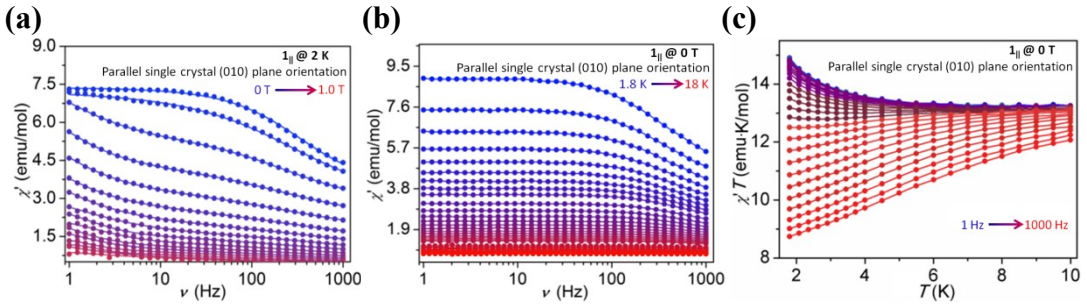

Figure S32. Variable-field χ_M' magnetic susceptibility versus frequency data for **1** (crystal layer) parallel single crystal (010) plane orientation, collected at fields ranging from 0 to 1 T at 2.0 K (a). Variable-temperature χ_M' magnetic susceptibility versus frequency data (b) variable-frequency $\chi_M'T$ magnetic susceptibility versus temperature data (c) for compound **1**, perpendicular single crystal (010) plane orientation under zero applied dc field, collected at temperatures ranging from 1.8 to 20.0 K and frequencies from 1.0 to 1000 Hz, respectively.

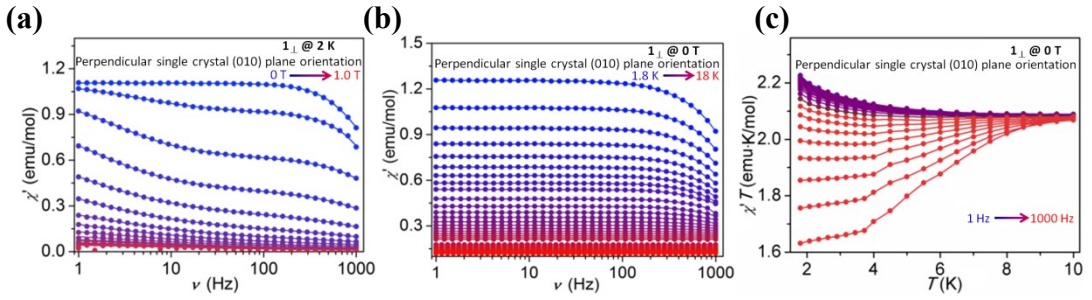

Figure S33. Variable-field χ_M' magnetic susceptibility versus frequency data for **1** (crystal layer) perpendicular single crystal (010) plane orientation, collected at fields ranging from 0 to 1 T at 2.0 K (a). Variable-temperature χ_M' magnetic susceptibility versus frequency data (b) variable-frequency $\chi_M'T$ magnetic susceptibility versus temperature data (c) for compound **1**, perpendicular single crystal (010) plane orientation under zero applied dc field, collected at temperatures ranging from 1.8 to 20.0 K and frequencies from 1.0 to 1000 Hz, respectively.

Table S7. Results obtained from the fitting of the frequency-dependent *ac* susceptibility for compound **1** on a randomly oriented powder sample under zero applied dc field.

Medium relaxation					
Magnetic relaxation pathway	τ_{QTM} **(s)**	C **($s^{-1}K^{-n}$)**	n	τ_0 **(s)**	U_{eff} **(K)**
Orbach process	---	---	---	6.48(4)E-7	56.15(9)
Raman process	---	3.91(3)E-3	1.57(6)	---	---
QTM process	2.08(6)E-2	---	---	---	---
QTM, Orbach and Raman processes	1.09(3)E-2	2.26(6)E-3	2.14(2)	7.46(5)E-6	41.08(1)
Faster relaxation					
Magnetic relaxation pathway	τ_{QTM} **(s)**	C **($s^{-1}K^{-n}$)**	n	τ_0 **(s)**	U_{eff} **(K)**
Orbach process	---	---	---	5.24(6)E-6	38.15(1)
Raman process	---	2.01(7)E-3	1.34(4)	---	---
QTM process	3.60(9)E-3	---	---	---	---
QTM, Orbach and Raman processes	2.75(4)E-3	1.98(1)E-3	1.63(5)	9.86(4)E-6	30.59(2)

Table S8. Results obtained from the fitting of the frequency-dependent *ac* susceptibility for compound **1-$Dy_{0.50}Y_{0.50}$** on a randomly oriented powder sample under zero applied dc field.

Magnetic relaxation pathway	τ_{QTM} **(s)**	C **($s^{-1}K^{-n}$)**	n	τ_0 **(s)**	U_{eff} **(K)**
Orbach process	---	---	---	2.52(3)E-11	156.81(9)
Raman process	---	1.91(7)E-3	9.26(4)	---	---
QTM process	4.28(2)E-3	---	---	---	---
QTM, Orbach and Raman processes	2.94(6)E-3	1.54(9)E-3	7.83(2)	8.06(4)E-10	124.62(5)

Table S9. Results obtained from the fitting of the frequency-dependent *ac* susceptibility for compound **1-$Dy_{0.10}Y_{0.90}$** on a randomly oriented powder sample under zero applied dc field.

Magnetic relaxation pathway	τ_{QTM} (s)	C ($s^{-1}K^{-n}$)	n	τ_0 (s)	U_{eff} (K)
Orbach process	---	---	---	1.65(8)E-11	176.20(3)
Raman process	---	1.31(5)E-4	7.68(3)	---	---
QTM process	8.59(1)E-3	---	---	---	---
QTM, Orbach and Raman processes	6.02(4)E-3	1.08(2)E-4	6.94(1)	8.12(9)E-10	149.18(6)

Table S10. Results obtained from the fitting of the frequency-dependent *ac* susceptibility for compound **1**, parallel single crystal (010) plane orientation under zero applied dc field.

Medium relaxation					
Magnetic relaxation pathway	**τ_{QTM} (s)**	**C ($s^{-1}K^{-n}$)**	**n**	**τ_0 (s)**	**U_{eff} (K)**
Orbach process	---	---	---	5.18(4)E-7	68.33(9)
Raman process	---	6.19(1)E-3	1.34(4)	---	---
QTM process	7.21(5)E-2	---	---	---	---
QTM, Orbach and Raman processes	4.83(6)E-2	4.54(9)E-3	3.18(4)	5.02(3)E-6	43.15(6)

Table S11. Results obtained from the fitting of the frequency-dependent *ac* susceptibility for compound **1**, perpendicular single crystal (010) plane orientation under zero applied dc field.

Magnetic relaxation pathway	τ_{QTM} (s)	C ($s^{-1}K^{-n}$)	n
Raman process	---	9.03(5)E-2	4.62(9)
QTM process	6.26(3)E-2	---	---
QTM and Raman processes	2.09(1)E-2	6.14(2)E-2	5.52(8)

Table S12. Magnetization relaxation fitting parameters from least-squares fitting of $\chi(\omega)$ data for compound **1** (powder sample) at 2.0 K and various dc fields.

	SR				FR		
***H* (Oe)**	$\chi_{s,\,tot}$	$\Delta\chi_1$	α_1	τ_1 / s	$\Delta\chi_2$	α_2	τ_2 / s
0	0.750(6)	---	---	---	-0.497(8)	0.231(7)	0.0412(6)
200	0.748(4)	5.230(4)	0.447(1)	0.0424(8)	-0.627(6)	0.228(9)	0.0404(1)
400	0.739(2)	5.220(1)	0.443(4)	0.0441(2)	-0.738(4)	0.228(6)	0.0394(5)
600	0.728(2)	5.110(6)	0.438(3)	0.0461(4)	-0.819(2)	0.228(2)	0.0389(4)
800	0.723(5)	5.102(5)	0.437(1)	0.0485(3)	-0.842(8)	0.224(5)	0.0384(7)
1000	0.707(5)	5.076(1)	0.435(4)	0.0514(9)	-0.906(4)	0.208(2)	0.0380(2)
1200	0.668(1)	4.961(7)	0.424(6)	0.0532(9)	-0.996(3)	0.205(2)	0.0376(9)
1400	0.636(4)	4.947(4)	0.418(1)	0.0562(8)	-1.032(5)	0.202(4)	0.0371(6)
1600	0.621(2)	4.877(1)	0.410(2)	0.0595(3)	-1.090(8)	0.195(9)	0.0365(1)
1800	0.604(1)	4.800(8)	0.399(2)	0.0619(3)	-1.151(7)	0.194(1)	0.0360(4)
2000	0.600(8)	4.777(3)	0.397(1)	0.0641(2)	-1.242(1)	0.193(1)	0.0357(3)
2200	0.589(1)	4.736(8)	0.394(1)	0.0664(7)	-1.306(8)	0.188(4)	0.0353(6)
2400	0.576(6)	4.694(4)	0.381(1)	0.0685(8)	-1.364(4)	0.187(4)	0.0349(3)
2600	0.566(3)	4.672(8)	0.373(2)	0.0703(7)	-1.414(6)	0.169(1)	0.0346(9)
2800	0.557(4)	4.629(1)	0.339(1)	0.0715(1)	-1.479(4)	0.166(3)	0.0345(6)
3000	0.551(8)	4.588(9)	0.321(3)	0.0725(3)	-1.537(2)	0.156(6)	0.0343(4)
3200	0.546(2)	4.578(7)	0.314(2)	0.0730(7)	-1.590(8)	0.148(1)	0.0342(3)
3400	0.546(1)	4.557(1)	0.313(3)	0.0735(2)	-1.614(2)	0.141(3)	0.0341(3)
3600	0.542(2)	4.514(3)	0.277(2)	0.0727(1)	-1.620(7)	0.139(4)	0.0341(8)
3800	0.540(6)	4.494(7)	0.264(5)	0.0714(5)	-1.648(1)	0.138(1)	0.0343(7)
4000	0.539(9)	4.462(1)	0.227(1)	0.0691(4)	-1.663(9)	0.137(4)	0.0341(4)
4200	0.537(1)	4.441(3)	0.218(9)	0.0676(1)	-1.676(2)	0.135(6)	0.0339(7)
4400	0.535(5)	4.424(6)	0.194(7)	0.0657(9)	-1.686(4)	0.131(3)	0.0339(2)
4600	0.533(6)	4.406(1)	0.194(6)	0.0642(6)	-1.696(1)	0.123(2)	0.0338(3)
4800	0.532(5)	4.394(4)	0.182(8)	0.0627(3)	-1.710(3)	0.122(8)	0.0339(2)
5000	0.528(7)	4.383(1)	0.181(1)	0.0608(3)	-1.722(5)	0.117(4)	0.0340(2)
5200	0.528(5)	4.371(1)	0.160(5)	0.0588(6)	-1.729(9)	0.108(5)	0.0341(1)
5400	0.528(1)	4.361(5)	0.128(4)	0.0571(4)	-1.731(6)	0.098(7)	0.0338(6)
5600	0.516(2)	4.340(3)	0.077(4)	0.0557(8)	-1.736(1)	0.096(3)	0.0335(6)
5800	0.504(6)	4.334(8)	0.076(9)	0.0548(4)	-1.736(4)	0.094(3)	0.0336(5)
6000	0.494(8)	4.324(2)	0.075(1)	0.0535(5)	-1.740(5)	0.088(8)	0.0334(8)
6200	0.494(1)	4.322(1)	0.069(4)	0.0527(8)	-1.743(9)	0.088(9)	0.0336(1)
6400	0.484(7)	4.318(6)	0.067(9)	0.0510(8)	-1.7450(9)	0.082(1)	0.0338(2)
6600	0.474(1)	4.308(7)	0.065(1)	0.0498(1)	-1.753(2)	0.079(7)	0.0337(4)
6800	0.450(1)	4.306(6)	0.062(3)	0.0499(2)	-1.759(2)	0.079(1)	0.0339(3)
7000	0.446(8)	4.302(5)	0.060(2)	0.0506(4)	-1.762(8)	0.075(3)	0.0341(5)

7200	0.427(6)	4.283(4)	0.056(3)	0.0516(8)	-1.764(6)	0.072(5)	0.0337(8)
7400	0.426(8)	4.280(2)	0.056(1)	0.0526(5)	-1.769(6)	0.071(9)	0.0337(7)
7600	0.424(1)	4.277(7)	0.052(1)	0.0536(1)	-1.769(7)	0.067(1)	0.0337(1)
7800	0.416(5)	4.272(4)	0.048(9)	0.0562(9)	-1.769(7)	0.065(6)	0.0335(3)
8000	0.412(1)	4.271(9)	0.044(5)	0.0580(6)	-1.770(5)	0.060(5)	0.0334(1)
8200	0.401(5)	4.271(1)	0.042(9)	0.0613(2)	-1.770(6)	0.056(4)	0.0334(8)
8400	0.391(2)	4.264(4)	0.042(4)	0.0625(4)	-1.771(6)	0.051(3)	0.0334(4)
8600	0.389(1)	4.254(2)	0.039(6)	0.0616(3)	-1.771(7)	0.044(9)	0.0331(5)
8800	0.384(8)	4.251(1)	0.038(6)	0.0564(2)	-1.775(7)	0.044(6)	0.0329(9)
9000	0.371(1)	4.249(1)	0.038(3)	0.0491(4)	-1.775(8)	0.029(5)	0.0328(4)
9200	0.345(1)	4.249(1)	0.037(3)	0.0410(9)	-1.775(9)	0.010(6)	0.0327(5)
9400	0.321(9)	4.247(6)	0.036(8)	0.0330(2)	-1.776(8)	0.010(5)	0.0326(9)
9600	0.310(3)	4.245(2)	0.035(8)	0.0325(4)	-1.777(2)	0.008(1)	0.0326(1)
9800	0.306(5)	4.243(9)	0.034(9)	0.0320(8)	-1.779(4)	0.003(5)	0.0322(6)
10000	0.296(9)	4.242(5)	0.018(6)	0.0316(4)	-1.780(1)	0.001(6)	0.0319(3)

Table S13. Magnetization relaxation fitting parameters from least-squares fitting of $\chi(\omega)$ data for compound **1** (powder sample) under zero-dc field.

			MR			FR	
T (K)	$\chi_{s,\,tot}$	$\Delta\chi_1$	α_1	τ_1 / s	$\Delta\chi_2$	α_2	τ_2 / s
1.8	1.433(5)	3.925(1)	0.523(4)	0.0259(5)	2.358(9)	0.076(5)	0.0034(1)
2.0	1.312(7)	3.174(2)	0.500(6)	0.0249(1)	1.871(3)	0.117(2)	0.0032(7)
2.3	1.207(8)	2.549(5)	0.464(2)	0.0241(7)	1.671(3)	0.211(5)	0.0031(5)
2.6	1.056(5)	2.438(9)	0.494(3)	0.0244(1)	1.153(1)	0.180(1)	0.0029(8)
2.9	0.938(7)	1.874(5)	0.430(1)	0.0227(6)	1.162(6)	0.256(5)	0.0028(7)
3.2	0.817(1)	1.671(6)	0.421(2)	0.0216(2)	0.997(9)	0.245(2)	0.0027(1)
3.5	0.744(3)	1.389(4)	0.382(1)	0.0212(4)	0.956(1)	0.266(9)	0.0025(6)
3.7	0.655(6)	1.268(7)	0.376(1)	0.0207(8)	0.845(2)	0.250(2)	0.0024(6)
4.0	0.590(6)	1.237(8)	0.393(9)	0.0201(1)	0.697(1)	0.214(1)	0.0021(5)
4.5	0.461(2)	1.062(8)	0.380(4)	0.0190(8)	0.586(4)	0.198(4)	0.0019(2)
5.0	0.375(1)	0.962(1)	0.382(1)	0.0184(5)	0.475(8)	0.170(9)	0.0017(8)
5.5	0.275(8)	0.813(5)	0.350(7)	0.0170(6)	0.430(4)	0.170(2)	0.0016(5)
6.0	0.177(8)	0.732(9)	0.342(8)	0.0158(8)	0.369(4)	0.157(5)	0.0016(1)
6.5	0.062(1)	0.649(4)	0.324(6)	0.0147(7)	0.324(5)	0.145(3)	0.0015(2)
7.0	-0.013(7)	0.585(4)	0.312(1)	0.0135(9)	0.287(9)	0.141(4)	0.0014(4)
7.5	-0.061(9)	0.532(1)	0.303(2)	0.0128(5)	0.259(8)	0.137(9)	0.0013(9)
8.0	-0.113(2)	0.482(3)	0.289(1)	0.0121(9)	0.235(6)	0.133(1)	0.0013(3)
8.5	-0.164(7)	0.426(1)	0.259(9)	0.0116(1)	0.212(2)	0.122(5)	0.0012(7)
9.0	-0.200(3)	0.396(8)	0.255(7)	0.0104(9)	0.192(9)	0.115(8)	0.0011(7)
9.5	-0.235(4)	0.347(2)	0.220(1)	0.0080(8)	0.179(3)	0.106(5)	0.0010(1)
10.0	-0.261(6)	0.323(1)	0.213(6)	0.0064(1)	0.161(5)	0.098(1)	8.6336(8)E-4
11.0	-0.339(5)	0.231(6)	0.176(4)	0.0045(6)	0.130(1)	0.096(9)	6.0244(8)E-4
12.0	-0.367(7)	0.173(3)	0.074(4)	0.0037(9)	0.120(9)	0.071(5)	4.9719(9)E-4
13.0	-0.393(9)	0.152(3)	0.061(7)	0.0031(2)	0.112(1)	0.073(5)	4.2499(2)E-4
14.0	-0.410(1)	0.146(5)	0.089(1)	0.0025(4)	0.096(8)	0.066(7)	3.5806(4)E-4
15.0	-0.426(9)	0.239(5)	0.247(4)	0.0021(1)	0.055(4)	0.033(4)	3.3035(6)E-4
16.0	-0.445(4)	0.236(5)	0.204(9)	0.0019(1)	0.040(5)	0.075(4)	3.0089(5)E-4
17.0	-0.457(5)	0.246(9)	0.202(4)	0.0016(9)	0.025(7)	0.125(2)	2.7170(1)E-4
18.0	1.433(5)	3.925(1)	0.523(4)	0.0015(9)	2.358(9)	0.076(5)	1.0506(9)E-4

Table S14. MagnetizationRelaxation fitting parameters from least-squares fitting of $\chi(\omega)$ data for diluted sample of **1-$Dy_{0.50}Y_{0.50}$** under zero dc field.

T	χ_T	χ_s	α	τ / s
1.8	5.595(2)	3.404(7)	0.434(8)	0.0026(4)
2.0	5.448(1)	3.551(8)	0.432(8)	0.0025(8)
2.3	5.336(1)	3.663(8)	0.431(9)	0.0025(3)
2.6	5.247(8)	3.752(1)	0.431(4)	0.0024(7)
2.9	5.175(9)	3.824(1)	0.430(8)	0.0024(1)
3.2	5.116(9)	3.883(1)	0.430(9)	0.0023(3)
3.5	5.065(8)	3.934(1)	0.429(7)	0.0022(5)
3.7	5.023(1)	3.976(8)	0.428(8)	0.0021(6)
4.0	4.984(7)	4.015(2)	0.424(1)	0.0020(6)
4.5	4.926(5)	4.073(4)	0.412(1)	0.0018(2)
5.0	4.881(1)	4.118(9)	0.400(1)	0.0015(1)
5.5	4.842(1)	4.157(9)	0.385(6)	0.0012(9)
6.0	4.804(4)	4.195(6)	0.358(4)	0.0010(1)
6.5	4.769(2)	4.230(7)	0.314(1)	8.2216(5)E-4
7.0	4.738(1)	4.261(9)	0.250(8)	6.3493(2)E-4
7.5	4.712(3)	4.287(6)	0.177(4)	4.4699(5)E-4
8.0	4.691(9)	4.308(1)	0.109(4)	2.8538(6)E-4
8.5	4.676(6)	4.323(3)	0.064(1)	1.7035(2)E-4
9.0	4.672(4)	4.327(5)	0.057(6)	9.1761(5)E-5
9.5	4.731(9)	4.268(1)	0.090(6)	3.2215(1)E-5
10.0	5.122(2)	4.877(7)	0.132(8)	2.2003(9)E-5

Table S15. Magnetization relaxation fitting parameters from least-squares fitting of $\chi(\omega)$ data for diluted sample of **1-Dy$_{0.10}$Y$_{0.90}$** under zero dc field.

T	χ_T	χ_s	α	τ / s
1.8	6.554(1)	5.445(9)	0.571(9)	0.0088(5)
2.0	6.480(9)	5.519(1)	0.572(2)	0.0086(6)
2.3	6.424(3)	5.575(7)	0.571(8)	0.0084(1)
2.6	6.379(3)	5.620(6)	0.571(8)	0.0081(6)
2.9	6.344(5)	5.655(4)	0.574(1)	0.0079(7)
3.2	6.315(1)	5.684(9)	0.575(1)	0.0077(8)
3.5	6.289(6)	5.710(3)	0.574(7)	0.0075(4)
3.7	6.269(8)	5.730(1)	0.576(5)	0.0074(1)
4.0	6.252(7)	5.747(2)	0.576(6)	0.0072(9)
4.5	6.226(5)	5.773(4)	0.571(1)	0.0070(2)
5.0	6.200(5)	5.799(4)	0.546(9)	0.0063(1)
5.5	6.173(1)	5.826(9)	0.496(1)	0.0051(4)
6.0	6.148(6)	5.851(3)	0.427(4)	0.0039(2)
6.5	6.130(5)	5.869(4)	0.355(8)	0.0027(8)
7.0	6.116(9)	5.883(1)	0.287(6)	0.0017(6)
7.5	6.107(5)	5.892(4)	0.235(3)	9.8706(5)E-4
8.0	6.102(7)	5.897(2)	0.216(1)	4.9534(1)E-4
8.5	6.109(1)	5.890(8)	0.255(8)	1.9918(9)E-4
9.0	6.199(5)	5.800(4)	0.375(1)	6.3955(6)E-5
9.5	6.842(8)	5.157(2)	0.454(6)	2.0786(1)E-5
10.0	6.835(2)	5.164(7)	0.481(3)	8.3086(4)E-6

Table S16. Magnetization relaxation fitting parameters from least-squares fitting of $\chi(\omega)$ data for compound **1** ($H_{|}$ 010) at 2.0 K and various dc fields.

				SR		MR	
***H* (Oe)**	$\chi_{s,\,tot}$	$\Delta\chi_1$	α_1	τ_1 / s	$\Delta\chi_2$	α_2	τ_2 / s
0	---	---	---	---	-1.756(1)	0.681(1)	0.0466(9)
600	0.168(1)	2.057(8)	0.651(2)	0.0546(5)	-1.769(5)	0.676(4)	0.0345(2)
1200	0.159(3)	2.044(9)	0.652(2)	0.0897(9)	-1.781(1)	0.675(3)	0.0322(1)
1800	0.153(1)	2.033(5)	0.653(1)	0.1266(1)	-1.791(3)	0.674(2)	0.0271(1)
2400	0.147(6)	2.022(7)	0.653(2)	0.1504(9)	-1.800(5)	0.672(5)	0.0229(5)
3000	0.142(4)	2.020(4)	0.653(9)	0.1662(6)	-1.802(7)	0.673(3)	0.0217(7)
3600	0.137(2)	2.015(6)	0.656(5)	0.1456(3)	-1.806(9)	0.675(1)	0.0196(7)
4200	0.132(5)	2.014(6)	0.663(5)	0.1215(9)	-1.807(7)	0.681(9)	0.0153(1)
4800	0.129(2)	2.015(9)	0.669(4)	0.1027(1)	-1.806(4)	0.688(3)	0.0143(4)
5400	0.124(2)	2.018(9)	0.679(2)	0.1167(9)	-1.803(6)	0.698(9)	0.0137(6)
6000	0.119(4)	1.971(3)	0.483(4)	0.1385(3)	-1.874(9)	0.495(3)	0.0130(9)
6600	0.115(9)	1.977(8)	0.385(7)	0.1516(6)	-1.899(7)	0.396(8)	0.0127(7)
7200	0.111(2)	7.197(5)	0.310(6)	0.1613(1)	-7.130(4)	0.313(4)	0.0111(5)
7800	0.092(9)	18.224(1)	0.282(1)	0.1399(5)	-18.160(6)	0.283(1)	0.0075(5)
8400	0.083(1)	18.229(6)	0.284(4)	0.1011(4)	-18.165(6)	0.285(2)	0.0037(6)
9000	0.074(6)	19.260(4)	0.283(1)	0.0956(1)	-17.620(2)	0.294(1)	0.0029(4)
9600	0.066(1)	18.808(1)	0.283(1)	0.0613(6)	-17.985(5)	0.289(2)	0.0020(9)
10200	0.056(3)	18.858(8)	0.284(1)	0.0588(9)	-17.939(1)	0.288(7)	0.0015(1)

Table S17. Magnetization relaxation fitting parameters from least-squares fitting of $\chi(\omega)$ data for compound **1** ($H_{\perp}010$) at 2.0 K and various dc fields.

				SR		MR	
***H* (Oe)**	$\chi_{s,\,tot}$	$\Delta\chi_1$	α_1	τ_1 / s	$\Delta\chi_2$	α_2	τ_2 / s
0	--	--	--	--	2.358(9)	0.076(5)	1.8851(5)E-4
600	1.312(7)	3.174(2)	0.500(6)	9.5319(6)E-4	1.871(3)	0.117(2)	1.3782(8)E-4
1200	1.207(8)	2.549(5)	0.464(2)	0.0019(1)	1.671(3)	0.211(5)	9.1693(3)E-5
1800	1.056(5)	2.438(9)	0.494(3)	0.0026(8)	1.153(1)	0.180(1)	7.3556(1)E-5
2400	0.938(7)	1.874(5)	0.430(1)	0.0037(3)	1.162(6)	0.256(5)	6.9479(6)E-5
3000	0.817(1)	1.671(6)	0.421(2)	0.0043(1)	0.997(9)	0.245(2)	5.1536(4)E-5
3600	0.744(3)	1.389(4)	0.382(1)	0.0053(6)	0.956(1)	0.266(9)	4.1389(9)E-5
4200	0.655(6)	1.268(7)	0.376(1)	0.0067(3)	0.845(2)	0.250(2)	3.1736(5)E-5
4800	0.590(6)	1.237(8)	0.393(9)	0.0076(9)	0.697(1)	0.214(1)	2.1787(6)E-5
5400	0.461(2)	1.062(8)	0.380(4)	0.0088(4)	0.586(4)	0.198(4)	1.1854(3)-5
6000	0.375(1)	0.962(1)	0.382(1)	0.0101(8)	0.475(8)	0.170(9)	9.2267(2)E-6
6600	0.275(8)	0.813(5)	0.350(7)	0.0125(8)	0.430(4)	0.170(2)	8.2693(9)E-6
7200	0.177(8)	0.732(9)	0.342(8)	0.0149(1)	0.369(4)	0.157(5)	6.2590(6)E-6
7800	0.062(1)	0.649(4)	0.324(6)	0.0165(5)	0.324(5)	0.145(3)	4.2752(5)E-6
8400	-0.013(7)	0.585(4)	0.312(1)	0.0199(1)	0.287(9)	0.141(4)	2.2749(6)E-6
9000	-0.061(9)	0.532(1)	0.303(2)	0.0200(8)	0.259(8)	0.137(9)	1.3450(9)E-6
9600	-0.113(2)	0.482(3)	0.289(1)	0.0226(9)	0.235(6)	0.133(1)	9.9656(9)E-6
10200	-0.164(7)	0.426(1)	0.259(9)	0.0246(5)	0.212(2)	0.122(5)	8.2945(1)E-6

Table S18. Relaxation fitting parameters from least-squares fitting of $\chi(\omega)$ data for a magnetically oriented sample of **1** ($H_{\parallel}$ 010) under zero-dc field.

T	χ_T	χ_s	α	τ / s
1.8	5.261(4)	2.738(6)	0.205(5)	5.4969(9)E-4
2.0	5.018(8)	2.981(1)	0.197(1)	4.8791(6)E-4
2.3	4.849(7)	3.150(1)	0.189(2)	4.4472(5)E-4
2.6	4.727(4)	3.272(6)	0.183(4)	4.0820(1)E-4
2.9	4.627(4)	3.372(5)	0.172(9)	3.7990(1)E-4
3.2	4.556(8)	3.443(1)	0.170(9)	3.5120(2)E-4
3.5	4.494(3)	3.505(6)	0.165(8)	3.2839(9)E-4
3.7	4.442(2)	3.557(7)	0.157(9)	3.0529(9)E-4
4.0	4.401(6)	3.598(3)	0.155(8)	2.8516(4)E-4
4.5	4.340(6)	3.659(3)	0.148(1)	2.5201(3)E-4
5.0	4.290(1)	3.710(1)	0.136(3)	2.2490(1)E-4
5.5	4.252(7)	3.747(3)	0.130(3)	2.0325(6)E-4
6.0	4.219(5)	3.780(4)	0.115(1)	1.8400(1)E-4
6.5	4.196(1)	3.903(9)	0.115(3)	1.6799(9)E-4
7.0	4.180(4)	3.819(5)	0.126(1)	1.5475(2)E-4
7.5	4.161(5)	3.838(4)	0.115(1)	1.4143(1)E-4
8.0	4.144(4)	3.855(5)	0.101(1)	1.3026(3)E-4
8.5	4.133(3)	3.866(6)	0.095(1)	1.2075(6)E-4
9.0	4.120(1)	3.879(8)	0.093(8)	1.1329(8)E-4
9.5	4.107(8)	3.892(2)	0.092(2)	1.0605(3)E-4
10.0	4.104(1)	3.895(9)	0.104(7)	9.6100(1)E-5
12.0	4.075(8)	3.924(1)	0.078(3)	7.7610(3)E-5
13.0	4.063(6)	3.936(3)	0.066(3)	7.2790(1)E-5
14.0	4.072(8)	3.927(1)	0.136(9)	6.5759(9)E-5
15.0	4.043(3)	3.956(6)	0.023(1)	5.6649(9)E-5
16.0	4.057(2)	3.942(7)	0.119(3)	5.2320(1)E-5
17.0	4.032(3)	3.967(6)	0.032(1)	4.7350(2)E-5
18.0	4.032(9)	3.967(1)	0.051(7)	4.0770(2)E-5

Table S19. Relaxation fitting parameters from least-squares fitting of $\chi(\omega)$ data for a magnetically oriented sample of **1** ($H_{\perp}010$) under Hzero-dc field.

T	χ_T	χ_s	α	τ / s
1.8	9.144(6)	3.163(2)	0.112(7)	1.0314(3)E-4
2.0	7.547(3)	2.054(8)	0.100(7)	1.0159(9)E-4
2.3	5.733(1)	1.266(9)	0.091(7)	1.0068(1)E-4
2.6	3.170(2)	0.982(9)	0.083(9)	9.9723(2)E-5
2.9	2.436(6)	0.756(3)	0.077(5)	9.9279(8)E-5
3.2	1.910(9)	0.040(8)	0.071(6)	9.8976(2)E-5
3.5	0.680(4)	-0.195(4)	0.066(7)	9.7934(6)E-5
3.7	0.313(1)	-0.686(9)	0.062(7)	9.6634(8)E-5
4.0	-0.458(3)	-1.541(6)	0.056(8)	9.8729(3)E-5
4.5	-1.871(1)	-2.896(4)	0.059(7)	8.4558(6)E-5
5.0	-2.382(9)	-3.617(1)	0.048(2)	8.6375(1)E-5
5.5	-3.184(5)	-4.815(4)	0.043(7)	8.2486(1)E-5
6.0	-4.046(5)	-5.953(4)	0.044(1)	7.4755(3)E-5
6.5	-5.007(6)	-6.992(3)	0.046(1)	6.7439(1)E-5
7.0	-6.016(9)	-7.983(1)	0.047(5)	6.1308(1)E-5
7.5	-7.249(2)	-8.750(7)	0.050(4)	5.5986(7)E-5
8.0	-8.111(1)	-9.888(9)	0.057(1)	4.9171(9)E-5
8.5	-9.660(8)	-10.833(9)	0.064(4)	4.5443(7)E-5
9.0	-10.556(1)	-11.443(8)	0.072(5)	4.6921(8)E-5
9.5	-11.384(8)	-12.615(9)	0.086(1)	4.6076(1)E-5
10.0	-12.108(7)	-13.819(2)	0.096(4)	5.324(5)E-5
12.0	-13.208(3)	-14.791(6)	0.157(1)	6.8465(9)E-5
13.0	-14.604(8)	-15.395(1)	0.118(4)	1.1867(2)E-4
14.0	-15.368(3)	-16.631(6)	0.116(1)	1.4646(6)E-4
15.0	-16.266(2)	-17.733(7)	0.106(3)	1.5598(4)E-4
16.0	-17.204(1)	-18.795(9)	0.077(6)	1.7989(2)E-4
17.0	-18.119(8)	-19.880(1)	0.039(8)	2.3375(4)E-4
18.0	-19.075(6)	-20.924(3)	0.006(1)	2.6716(4)E-4

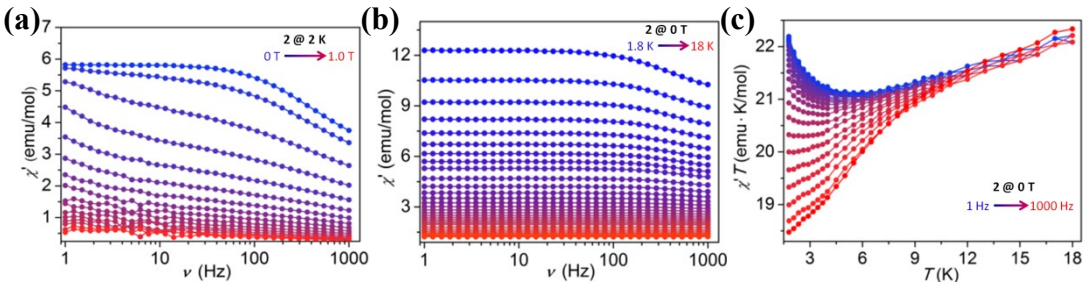

Figure S34. Variable-field χ_M' magnetic susceptibility versus frequency data for **2** (powder sample) on a random orientation, collected at fields ranging from 0 to 1 T at 2.0 K (a). Variable-temperature χ_M' magnetic susceptibility versus frequency data (b) variable-frequency $\chi_M'T$ magnetic susceptibility versus temperature data (c) for compound **2** on a randomly oriented powder sample under zero applied dc field, collected at temperatures ranging from 1.8 to 20.0 K and frequencies from 1.0 to 1000 Hz, respectively.

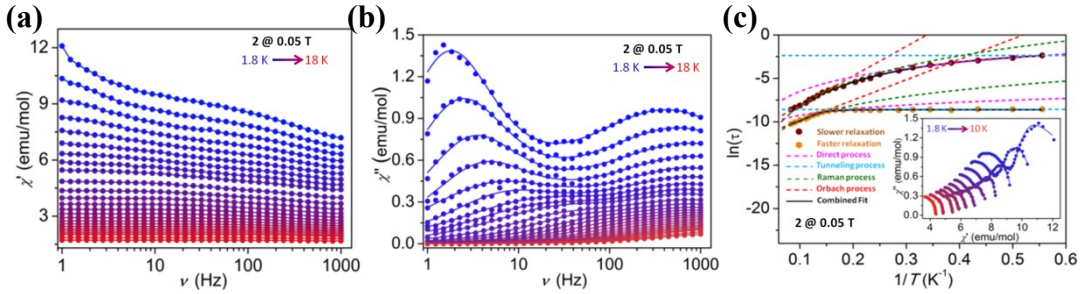

Figure S35. Variable-temperature χ_M' (a) and χ_M'' (b) magnetic susceptibility versus frequency data for **2** (powder sample) on a random orientation, collected at temperatures ranging from 1.8 to 20.0 K under 500 Oe dc field. Plot of inverse temperature versus the natural log of the magnetization relaxation time (c). Cole-Cole plots (c, inset). Magnetization relaxation time was extracted from the least-squares fitting using a generalized Debye model (Table S21). The best-fit parameters are obtained by combining Obrach process, Raman process and quantum tunneling of the magnetization ($\tau^{-1} = \tau_0^{-1}\exp(-U_{eff}/k_BT) + CT^n + AT + \tau_{tunnel}^{-1}$) yields the best parameters with U_{eff} = 53.64(5) K (29.72(7) K), τ_o = 2.18(1) × 10^{-7} s (1.73(5) × 10^{-6} s), τ_{QTM} = 0.00391(3) s (0.00259(4) s), C = 0.00631(4) s^{-1} $K^{-5.68}$ (0.00415(8) s^{-1} $K^{-4.42}$), n = 5.68(1) (4.42(9)) corresponding to the SR (FR) phase (Table S27).

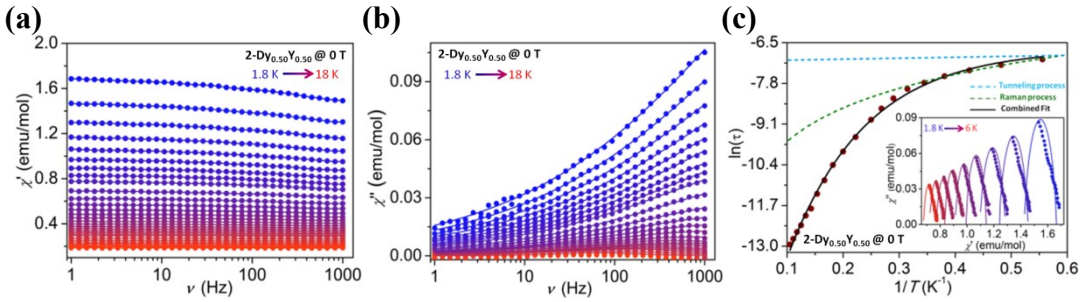

Figure S36. Variable-temperature χ_M' (a) and χ_M'' (b) magnetic susceptibility versus frequency data for **2-Dy$_{0.50}$Y$_{0.50}$** (powder sample) on a random orientation, collected at temperatures ranging from 1.8 to 20.0 K under zero applied dc field. Plot of inverse temperature versus the natural log of the magnetization relaxation time (c). Cole-Cole plots (c, inset). Magnetization relaxation time was extracted from the least-squares fitting using a generalized Debye model (Table S22). The best-fit parameters are obtained by combining Obrach process, Raman process and quantum tunneling of the magnetization ($\tau^{-1} = CT^n + \tau_{tunnel}^{-1}$) yields the best parameters with C = 0.00683(1) s^{-1} K$^{-3.03}$, n = 3.03(8), and τ_{tunnel} = 5.01(6) × 10^{-2} s (Table S28).

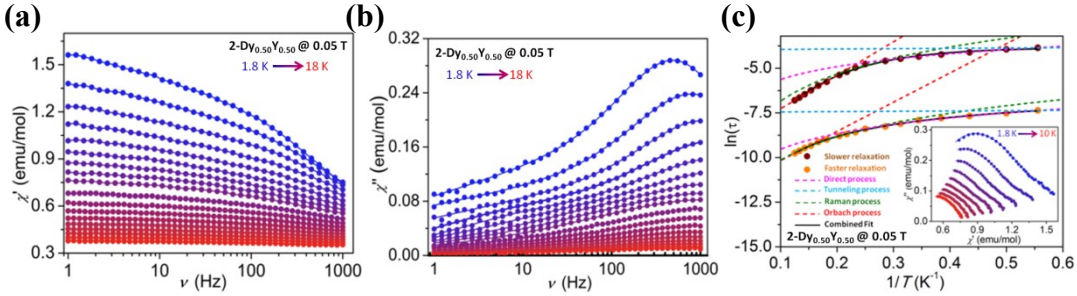

Figure S37. Variable-temperature χ_M' (a) and χ_M'' (b) magnetic susceptibility versus frequency data for **2-Dy$_{0.50}$Y$_{0.50}$** (powder sample) on a random orientation, collected at temperatures ranging from 1.8 to 20.0 K under 500 Oe dc field. Plot of inverse temperature versus the natural log of the magnetization relaxation time (c). Cole-Cole plots (c, inset). Magnetization relaxation time was extracted from the least-squares fitting using a generalized Debye model (Table S23). The best-fit parameters are obtained by combining Obrach process, Raman process and quantum tunneling of the magnetization ($\tau^{-1} = \tau_0^{-1}\exp(-U_{eff}/k_BT) + CT^n + AT + \tau_{tunnel}^{-1}$) yields the best parameters with U_{eff} = 20.13(9) K (15.67(5) K), τ_o = 9.08(6) × 10^{-7} s (1.04(1) × 10^{-6} s), τ_{QTM} = 0.00416(9) s (0.00011(7) s), C = 0.00857(3) s^{-1} K$^{-6.43}$ (0.00439(5) s^{-1} K$^{-4.91}$), n = 6.43(4) (4.91(3)) corresponding to the SR (FR) phase (Table S29).

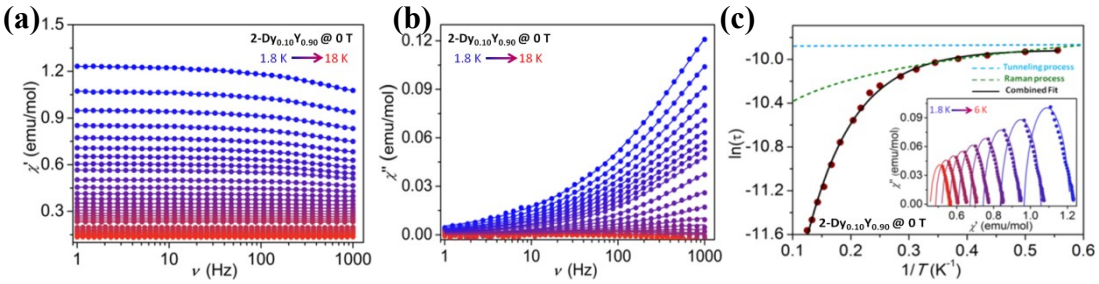

Figure S38. Variable-temperature χ_M' (a) and χ_M'' (b) magnetic susceptibility versus frequency data for **2-Dy$_{0.10}$Y$_{0.90}$** (powder sample) on a random orientation, collected at temperatures ranging from 1.8 to 20.0 K under zero applied dc field. Plot of inverse temperature versus the natural log of the magnetization relaxation time (c). Cole-Cole plots (c, inset). Magnetization relaxation time was extracted from the least-squares fitting using a generalized Debye model (Table S24). The best-fit parameters are obtained by combining Obrach process, Raman process and quantum tunneling of the magnetization ($\tau^{-1} = CT^n + \tau_{tunnel}^{-1}$) yields the best parameters with C = 0.00166(7) s^{-1} K$^{-2.87}$, n = 2.87(9), and τ_{tunnel} = 4.25(2) × 10^{-2} s (Table S30).

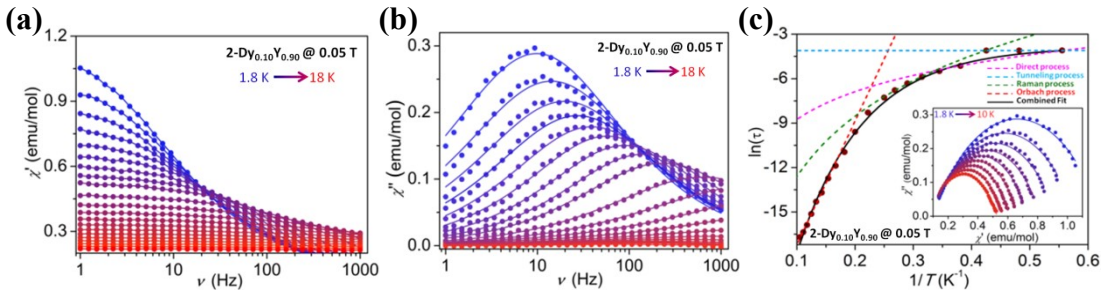

Figure S39. Variable-temperature χ_M' (a) and χ_M'' (b) magnetic susceptibility versus frequency data for **2-Dy$_{0.10}$Y$_{0.90}$** (powder sample) on a random orientation, collected at temperatures ranging from 1.8 to 20.0 K under 500 Oe dc field. Plot of inverse temperature versus the natural log of the magnetization relaxation time (c). Cole-Cole plots (c, inset). Magnetization relaxation time was extracted from the least-squares fitting using a generalized Debye model (Table S25). The best-fit parameters are obtained by combining Obrach process, Raman process and quantum tunneling of the magnetization ($\tau^{-1} = \tau_0^{-1}\exp(-U_{eff}/k_BT) + CT^n + AT + \tau_{tunnel}^{-1}$) yields the best parameters with U_{eff} = 87.31(6) K, τ_o = 6.23(1) × 10^{-8} s, C = 0.00045(8) s^{-1} K$^{-5.93}$, n = 5.93(4), and τ_{tunnel} = 8.95(5) × 10^{-4} s (Table S31).

Table S20. Results obtained from the fitting of the frequency-dependent *ac* susceptibility for compound **2** under zero dc field.

Slower relaxation					
Magnetic relaxation pathway	τ_{QTM} **(s)**	C **($s^{-1}K^{-n}$)**	n	τ_0 **(s)**	U_{eff} **(K)**
Orbach process	---	---	---	9.05(1)E-7	31.34(6)
Raman process	---	9.21(8)E-3	3.59(6)	---	---
QTM process	2.92(8)E-2	---	---	---	---
QTM, Orbach and Raman processes	3.01(1)E-2	2.09(4)E-3	4.36(9)	5.20(5)E-6	22.98(5)

Table S21. Results obtained from the fitting of the frequency-dependent *ac* susceptibility for compound **2** under the optimal 500 Oe static field.

Slower relaxation						
Magnetic relaxation pathway	τ_{QTM} **(s)**	C **($s^{-1}K^{-n}$)**	n	τ_0 **(s)**	U_{eff} **(K)**	A **($s^{-1}K^{-n}$)**
Direct process	---	---	---	---	---	4.01(5)E-3
Orbach process	---	---	---	9.25(6)E-7	66.33(8)	---
Raman process	---	8.75(5)E-3	4.11(3)	---	---	---
QTM process	2.56(3)E-2	---	---	---	---	---
Direct, QTM, Orbach and Raman processes	3.91(3)E-3	6.31(4)E-3	5.68(1)	2.18(1)E-7	53.64(5)	5.29(4)E-4
Faster relaxation						
Magnetic relaxation pathway	τ_{QTM} **(s)**	C **($s^{-1}K^{-n}$)**	n	τ_0 **(s)**	U_{eff} **(K)**	A **($s^{-1}K^{-n}$)**
Direct process	---	---	---	---	---	8.01(6)E-3
Orbach process	---	---	---	6.36(6)E-6	45.50(3)	---
Raman process	---	3.67(1)E-3	2.26(3)	---	---	---
QTM process	8.65(5)E-3	---	---	---	---	---
QTM, Orbach and Raman processes	2.59(4)E-3	4.15(8)E-3	4.42(9)	1.73(5)E-6	29.72(7)	7.76(1)E-4

Table S22. Results obtained from the fitting of the frequency-dependent *ac* susceptibility for diluted sample of compound **2-$Dy_{0.50}Y_{0.50}$** under zero-dc field.

Magnetic relaxation pathway	τ_{QTM} (s)	C ($s^{-1}K^{-n}$)	n
Raman process	---	4.45(3)	1.54(4)
QTM process	1.39(5)E-4	---	---
QTM and Raman processes	5.01(6)E-2	6.83(1)	3.03(8)

Table S23. Results obtained from the fitting of the frequency-dependent *ac* susceptibility for diluted sample of compound **2-$Dy_{0.50}Y_{0.50}$** under the optimal 500 Oe static field.

Slower relaxation						
Magnetic relaxation pathway	τ_{QTM} (s)	C ($s^{-1}K^{-n}$)	n	τ_0 (s)	U_{eff} (K)	A ($s^{-1}K^{-n}$)
Direct process	---	---	---	---	---	1.48(4)E-3
Orbach process	---	---	---	5.71(3)E-7	37.24(4)	---
Raman process	---	6.43(6)E-3	5.85(3)	---	---	---
QTM process	9.84(5)E-3	---	---	---	---	---
Direct, QTM, Orbach and Raman processes	4.16(9)E-3	8.57(3)E-3	6.43(4)	9.08(6)E-7	36.13(9)	2.25(3)E-4
Faster relaxation						
Magnetic relaxation pathway	τ_{QTM} (s)	C ($s^{-1}K^{-n}$)	n	τ_0 (s)	U_{eff} (K)	A ($s^{-1}K^{-n}$)
Direct process	---	---	---	---	---	1.75(4)E-3
Orbach process	---	---	---	8.48(4)E-6	29.61(9)	---
Raman process	---	2.62(4)E-3	3.63(7)	---	---	---
QTM process	3.37(1)E-3	---	---	---	---	---
QTM, Orbach and Raman processes	1.17(8)E-4	4.39(5)E-3	4.91(3)	1.04(1)E-6	15.67(5)	3.04(5)E-4

Table S24. Results obtained from the fitting of the frequency-dependent *ac* susceptibility for diluted sample of **2-Dy$_{0.10}$Y$_{0.90}$** under zero dc field.

Magnetic relaxation pathway	τ_{QTM} (s)	C ($s^{-1}K^{-n}$)	n
Raman process	---	1.32(9)	1.98(3)
QTM process	9.17(6)E-3	---	---
QTM and Raman processes	4.25(2)E-2	1.66(7)	2.87(9)

Table S25. Results obtained from the fitting of the frequency-dependent *ac* susceptibility for diluted sample of compound **2-Dy$_{0.10}$Y$_{0.90}$** under the optimal 500 Oe static field.

Slower relaxation						
Magnetic relaxation pathway	τ_{QTM} (s)	C ($s^{-1}K^{-n}$)	n	τ_0 (s)	U_{eff} (K)	A ($s^{-1}K^{-n}$)
Direct process	---	---	---	---	---	1.43(8)E-4
Orbach process	---	---	---	2.70(9)E-8	104.66(7)	---
Raman process	---	6.19(6)E-4	4.80(1)	---	---	---
QTM process	3.92(1)E-3	---	---	---	---	---
Direct, QTM, Orbach and Raman processes	8.95(5)E-4	4.58(7)E-4	5.93(4)	6.23(1)E-8	87.31(6)	5.89(9)E-4

Table S26. Magnetization relaxation fitting parameters from least-squares fitting of $\chi(\omega)$ data for compound **2** under zero dc field.

T	χ_T	χ_s	α	τ / s
1.8	19.185(6)	15.814(3)	0.181(7)	2.883(3)E-4
2.0	16.879(1)	14.120(8)	0.173(1)	2.624(3)E-4
2.3	15.162(3)	12.837(6)	0.1662(8)	2.451(7)E-4
2.6	13.500(5)	11.499(4)	0.159(9)	2.307(4)E-4
2.9	11.855(8)	10.144(1)	0.153(5)	2.254(5)E-4
3.2	10.249(7)	8.750(2)	0.147(9)	2.170(7)E-4
3.5	8.666(7)	7.333(2)	0.142(1)	2.084(9)
3.7	7.102(5)	5.897(4)	0.140(4)	1.979(6)E-4
4.0	5.544(2)	4.455(7)	0.134(7)	1.894(5)E-4
4.5	3.961(8)	3.038(1)	0.126(1)	1.727(1)E-4
5.0	2.896(1)	2.103(9)	0.118(4)	1.573(1)E-4
5.5	1.842(1)	1.157(8)	0.113(4)	1.432(3)E-4
6.0	1.046(4)	0.453(6)	0.106(1)	1.316(6)E-4
6.5	0.411(5)	-0.111(5)	0.107(8)	1.197(2)E-4
7.0	-0.520(8)	-0.979(1)	0.103(7)	1.111(8)E-4
7.5	-1.295(3)	-1.704(6)	0.108(6)	1.012(6)E-4
8.0	-2.321(5)	-2.678(4)	0.105(2)	9.683(3)E-5
8.5	-3.354(9)	-3.645(1)	0.119(1)	8.408(9)E-5
9.0	-4.371(7)	-4.628(2)	0.116(4)	8.211(2)E-5
9.5	-5.382(3)	-5.617(6)	0.114(1)	7.920(1)E-5
10.0	-6.389(1)	-6.610(8)	-0.135(6)	7.639(4)E-5
12.0	-7.408(2)	-7.591(7)	0.119(1)	7.338(8)E-5
13.0	-8.428(1)	-8.571(9)	0.115(3)	7.018(8)E-5
14.0	-9.435(9)	-9.564(1)	0.138(5)	6.891(7)E-5
15.0	-10.450(6)	-10.549(3)	0.108(6)	6.549(6)E-5
16.0	-11.450(1)	-11.549(9)	0.134(3)	6.322(9)E-5
17.0	-12.457(8)	-12.542(1)	0.122(9)	6.028(1)E-5
18.0	-13.465(8)	-13.534(2)	0.128(9)	5.676(5)E-5

Table S27. Relaxation fitting parameters from least-squares fitting of $\chi(\omega)$ data for compound **2** under the optimal 500 Oe static field.

			FR			SR	
T (K)	$\chi_{s,\,tot}$	$\Delta\chi_1$	α_1	τ_1 / s	$\Delta\chi_2$	α_2	τ_2 / s
1.8	-6.416(5)	4.202(6)	0.461(1)	1.912(4)E-4	2.815(1)	0.080(1)	0.094(7)
2.0	-5.512(8)	3.712(4)	0.471(3)	1.910(3)E-4	2.138(1)	0.102(9)	0.0705(8)
2.3	-4.490(1)	3.518(7)	0.509(6)	1.894(5)E-4	1.462(9)	0.093(6)	0.052(3)
2.6	-3.471(2)	2.991(5)	0.500(3)	1.864(6)E-4	1.096(1)	0.113(5)	0.040(4)
2.9	-2.355(2)	2.098(6)	0.412(8)	1.833(9)E-4	1.121(7)	0.266(9)	0.031(1)
3.2	-1.677(6)	2.064(5)	0.458(4)	1.815(4)E-4	0.724(1)	0.177(8)	0.023(1)
3.5	-1.106(9)	1.354(4)	0.336(9)	1.742(5)E-4	0.861(1)	0.315(8)	0.016(3)
3.7	-0.676(4)	1.331(9)	0.371(1)	1.735(5)E-4	0.649(7)	0.281(8)	0.010(6)
4.0	-0.295(6)	1.046(1)	0.276(5)	1.729(5)E-4	0.636(6)	0.304(6)	0.006(8)
4.5	0.624(8)	1.289(7)	0.439(4)	1.726(2)E-4	0.261(7)	0.138(7)	0.005(7)
5.0	1.545(3)	1.061(6)	0.394(1)	1.719(1)E-4	0.224(1)	0.090(1)	0.004(4)
5.5	2.361(2)	0.728(9)	0.285(1)	1.701(5)E-4	0.317(4)	0.203(1)	0.002(7)
6.0	3.152(8)	0.771(8)	0.316(3)	1.693(3)E-4	0.152(8)	0.039(3)	0.002(1)
6.5	4.570(3)	0.590(8)	0.234(1)	1.550(1)E-4	0.188(9)	0.112(7)	0.001(6)
7.0	5.551(5)	0.495(8)	0.203(3)	1.365(2)E-4	0.193(8)	0.153(5)	9.164(5)E-4
7.5	6.511(4)	0.417(6)	0.165(1)	1.109(9)E-4	0.200(7)	0.150(8)	6.850(6)E-4
8.0	7.830(6)	0.340(9)	0.118(1)	9.572(8)E-5	0.207(5)	0.156(3)	5.750(8)E-4
8.5	8.836(1)	0.292(5)	0.107(3)	7.963(9)E-5	0.189(3)	0.177(4)	3.952(4)E-4
9.0	9.549(5)	0.114(1)	0.201(6)	6.423(2)E-5	0.245(8)	0.158(7)	2.948(6)E-4
9.5	10.143(9)	0.091(5)	0.069(1)	5.473(5)E-5	0.135(3)	0.124(9)	2.326(4)E-4
10.0	11.182(7)	0.063(3)	0.204(9)	4.250(1)E-5	0.029(3)	0.073(9)	1.842(9)E-4
12.0	12.922(9)	0.033(5)	0.207(6)	3.497(1)E-5	0.019(1)	0.308(6)	1.051(6)E-4

Table S28. Magnetization relaxation fitting parameters from least-squares fitting of $\chi(\omega)$ data for diluted sample of compound **2-Dy$_{0.50}$Y$_{0.50}$** under zero-dc field.

T	χ_T	χ_s	α	τ / s
1.8	13.130(4)	11.867(8)	0.669(6)	8.805(1)E-4
2.0	13.025(8)	11.972(4)	0.667(6)	7.354(6)E-4
2.3	12.915(1)	12.083(2)	0.659(8)	6.211(1)E-4
2.6	12.862(5)	12.135(7)	0.660(6)	5.156(9)E-4
2.9	12.800(6)	12.197(6)	0.651(9)	4.171(6)E-4
3.2	12.755(6)	12.242(8)	0.645(2)	3.436(1)E-4
3.5	12.703(1)	12.295(1)	0.633(1)	2.540(4)E-4
3.7	12.681(4)	12.316(8)	0.627(1)	1.830(1)E-4
4.0	12.656(4)	12.341(8)	0.617(1)	1.278(1)E-4
4.5	12.623(1)	12.375(1)	0.610(1)	7.373(6)E-5
5.0	12.587(2)	12.411(1)	0.606(5)	4.640(9)E-5
5.5	12.561(4)	12.436(8)	0.585(9)	3.015(8)E-5
6.0	12.546(6)	12.451(6)	0.575(1)	1.851(3)E-5
6.5	12.537(6)	12.460(6)	0.585(2)	1.199(5)E-5
7.0	12.526(4)	12.471(8)	0.562(3)	7.511(6)E-6
7.5	12.517(9)	12.480(3)	0.494(8)	5.986(5)E-6
8.0	12.516(9)	12.481(3)	0.548(1)	4.403(9)E-6
8.5	12.512(3)	12.486(1)	0.478(4)	3.552(1)E-6
9.0	12.508(9)	12.489(3)	0.416(2)	2.859(1)E-6
9.5	12.506(2)	12.491(1)	0.410(9)	2.383(6)E-6

Table S29. Magnetization relaxation fitting parameters from least-squares fitting of $\chi(\omega)$ data for diluted sample of compound **2-Dy$_{0.50}$Y$_{0.50}$** under the optimal 500 Oe static field.

		FR			SR		
T **(K)**	$\chi_{s,\,tot}$	$\Delta\chi_1$	α_1	τ_1 / s	$\Delta\chi_2$	α_2	τ_2 / s
1.8	0.397(8)	0.690(4)	0.268(4)	6.342(9)E-4	0.694(5)	0.636(2)	0.021(1)
2.0	0.376(2)	0.634(2)	0.311(3)	5.426(5)E-4	0.623(6)	0.682(4)	0.019(3)
2.3	0.350(4)	0.438(3)	0.339(1)	4.642(9)E-4	0.574(3)	0.625(2)	0.016(4)
2.6	0.317(9)	0.187(9)	0.465(2)	4.116(9)E-4	0.733(8)	0.444(9)	0.014(5)
2.9	0.302(9)	0.113(7)	0.522(6)	3.655(8)E-4	0.728(1)	0.358(7)	0.012(9)
3.2	0.281(8)	0.262(1)	0.382(1)	3.014(2)E-4	0.382(1)	0.538(6)	0.011(5)
3.5	0.275(9)	0.480(4)	0.006(8)	2.568(5)E-4	0.055(9)	0.588(6)	0.010(1)
3.7	0.259(1)	0.468(6)	0.213(1)	2.257(6)E-4	0.051(5)	0.603(1)	0.008(5)
4.0	0.244(3)	0.449(9)	0.393(4)	1.880(1)E-4	0.047(1)	0.615(1)	0.006(9)
4.5	0.222(6)	0.417(1)	0.305(8)	1.691(1)E-4	0.031(9)	0.636(6)	0.005(5)
5.0	0.205(5)	0.375(3)	0.224(1)	1.527(1)E-4	0.027(1)	0.664(3)	0.004(5)
5.5	0.193(6)	0.304(4)	0.467(2)	1.246(5)E-4	0.011(4)	0.621(4)	0.003(1)
6.0	0.173(2)	0.200(9)	0.002(4)	1.080(4)E-4	-0.014(3)	0.579(8)	0.002(5)
6.5	0.165(3)	0.193(7)	0.111(1)	8.810(3)E-5	-0.028(8)	0.637(4)	0.001(9)
7.0	0.158(9)	0.137(3)	0.290(1)	7.705(4)E-5	-0.029(1)	0.592(9)	0.001(5)
7.5	0.146(4)	0.118(1)	0.029(9)	6.572(7)E-5	-0.052(2)	0.656(8)	0.001(2)
8.0	0.131(1)	0.100(9)	0.110(1)	5.754(1)E-5	-0.065(3)	0.750(6)	0.001(1)

Table S30. Magnetization relaxation fitting parameters from least-squares fitting of $\chi(\omega)$ data for diluted sample of **2-Dy$_{0.10}$Y$_{0.90}$** under zero dc field.

T	χ_T	χ_s	α	τ / s
1.8	12.860(5)	12.139(4)	0.476(1)	4.932(8)E-5
2.0	12.789(3)	12.210(6)	0.462(5)	4.864(3)E-5
2.3	12.740(7)	12.259(2)	0.450(3)	4.711(2)E-5
2.6	12.708(6)	12.291(3)	0.446(3)	4.567(3)E-5
2.9	12.674(7)	12.325(2)	0.433(3)	4.405(8)E-5
3.2	12.660(3)	12.339(6)	0.435(6)	4.140(9)E-5
3.5	12.632(3)	12.367(6)	0.408(4)	3.884(2)E-5
3.7	12.634(2)	12.365(7)	0.418(1)	3.567(6)E-5
4.0	12.614(6)	12.385(3)	0.394(9)	3.343(1)E-5
4.5	12.592(4)	12.407(5)	0.383(3)	2.915(1)E-5
5.0	12.625(9)	12.394(1)	0.478(8)	2.598(4)E-5
5.5	12.675(8)	12.324(1)	0.552(4)	2.127(4)E-5
6.0	12.560(1)	12.439(8)	0.574(2)	1.736(8)E-5
6.5	12.530(3)	12.469(6)	0.623(9)	1.416(5)E-5
7.0	12.511(3)	12.488(6)	0.620(9)	1.231(1)E-5
7.5	12.503(9)	12.496(1)	0.290(7)	1.046(9)E-5
8.0	12.501(9)	12.498(1)	0.077(1)	9.502(1)E-6

Table S31. Magnetization relaxation fitting parameters from least-squares fitting of $\chi(\omega)$ data for diluted sample of compound **2-$Dy_{0.10}Y_{0.90}$** under the optimal 500 Oe static field.

T	χ_T	χ_s	α	τ / s
1.8	13.048(3)	11.951(6)	0.383(2)	0.016(2)
2.0	12.971(2)	12.028(7)	0.385(1)	0.011(2)
2.3	12.908(6)	12.091(3)	0.379(1)	0.008(1)
2.6	12.858(8)	12.141(1)	0.365(5)	0.005(8)
2.9	12.817(4)	12.182(5)	0.347(6)	0.004(1)
3.2	12.758(1)	12.214(8)	0.334(1)	0.002(6)
3.5	12.758(7)	12.240(2)	0.331(5)	0.001(6)
3.7	12.738(1)	12.261(8)	0.334(2)	0.001(1)
4.0	12.723(6)	12.276(3)	0.355(9)	6.912(5)E-4
4.5	12.707(3)	12.292(6)	0.413(8)	2.512(6)E-4
5.0	12.710(4)	12.289(5)	0.485(1)	6.820(4)E-5
5.5	12.781(1)	12.218(9)	0.581(6)	1.743(5)E-5
6.0	12.767(3)	12.232(6)	0.634(6)	6.934(5)E-5
6.5	12.580(7)	12.419(2)	0.597(7)	2.952(1)E-6
7.0	12.538(9)	12.461(1)	0.555(5)	1.125(8)E-6
7.5	12.521(6)	12.478(3)	0.480(7)	6.135(5)E-7
8.0	12.516(6)	12.489(5)	0.415(9)	2.680(6)E-7
8.5	12.508(8)	12.491(1)	0.294(4)	1.280(3)E-7
9.0	12.506(1)	12.493(8)	0.286(8)	7.859(1)E-8
9.5	12.501(6)	12.496(6)	0.129(1)	5.616(3)E-8

S4 Magnetoluminescent

Photoluminescence of *f–f* electronic transitions is a useful technique for determining the magnetic energy levels of lanthanide compounds. Figure S40 and S41 depict the optical Photoluminescence of **1** and **1-Y**. The emission spectra is a broad peak of 440-700 nm, rather than three distinct emission components of Dy(III) compounds, preventing them from obtaining magnetic energy level parameters. In the magnetoluminescent measurement at 5 K, however, the intensity of the photoluminescence is dependent on the strength of the magnetic field in the range from 0 to 800 Oe. To better understand this phenomenon, the magnetoluminescence of diamagnetic **1-Y** was measured, and only magnetic independent photoluminescence is observed, indicating that the photoluminescence of **1** is derived from both the ligand and the *f–f* electronic transitions of Dy(III) ions. As a result, weak magnetic coupling may be responsible for the magnetic field-related intensity of photoluminescence in **1** in low magnetic field regime.

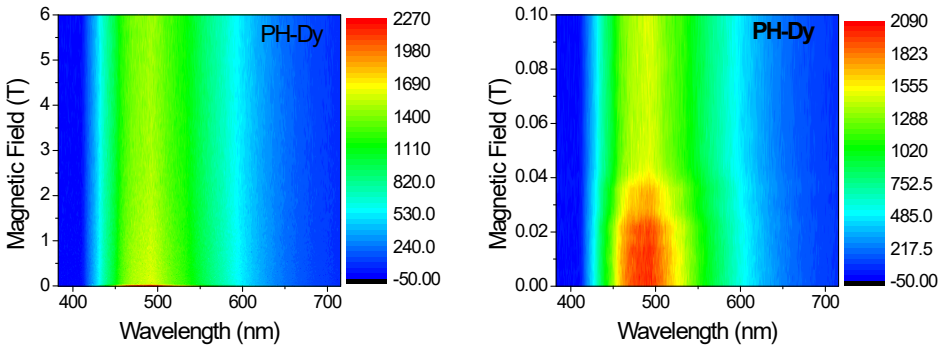

Figure S40. The luminescence spectrum (λ_{exc} = 402 nm) at 5 K under a pulsed magnetic field up to 6 T recorded in the range of 440–750 nm for **1**.

The spectrum revealed a clear signal in **1-Y**, which can be attributed to the photoluminescence of the ligand. The spectrum of **1** is similar to that of **1-Y**, and the emission peak is not shifted, indicating that the photoluminescence is primarily caused by the ligand. When a magnetic field was applied, the intensity of the emission

peak at 490 nm increased quickly and reached a maximum at 564 Oe, then decreased and became constant. This phenomenon was not observed in **1-Y**, implying the *f-f* electronic transitions of Dy(III) was also also exists, but it is very weak. Furthermore, the maximum intensity observed at 564 Oe may imply a energy level crossover point in the Zeeman split in the two dimension magnetic compound.

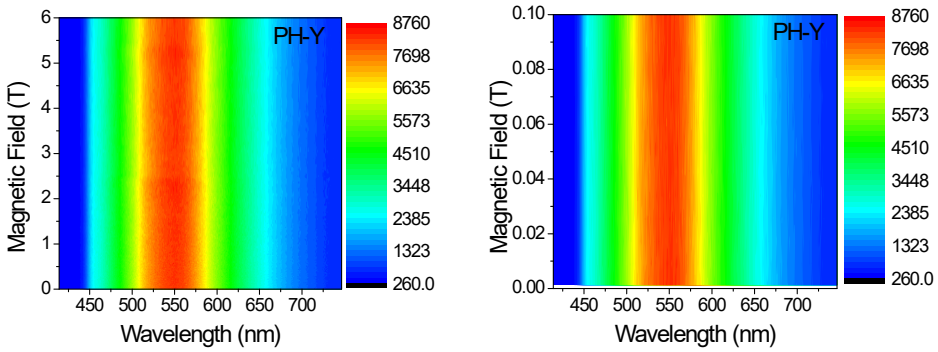

Figure S41. The luminescence spectrum (λ_{exc} = 402 nm) at 5 K under a pulsed magnetic field up to 6 T recorded in the range of 440–750 nm for **1-Y**.

S5 Theoretical Calculation

Complete-active-space self-consistent field (CASSCF) calculations were performed on individual Dy(III) fragment of **1** using OpenMolccas[S5] and SINGLE_ANISO[S6-S8] programs. Compound **1** is a two-dimensional chain including only one type of Dy(III) ion, thus we only need to calculate one Dy(III) fragment for it. Thus, a seven-core unit indicated as **[Dy]** was extracted from compound **1**. The influence of the nearest neighboring Dy(III) ions were taken into account by the closed-shell La^{III} *ab initio* embedding model potentials (La.EMB-AIMP.Sadoc.0s.0s.0e-La($LaMnO_3$). Complete-active-space self-consistent field (CASSCF) calculations on individual Dy(III) fragment of **[Dy]** (see Figure S42 for the calculated model structure) on the basis of single-crystal X-ray determined geometry have been carried out with OpenMolcas program package.[S9]

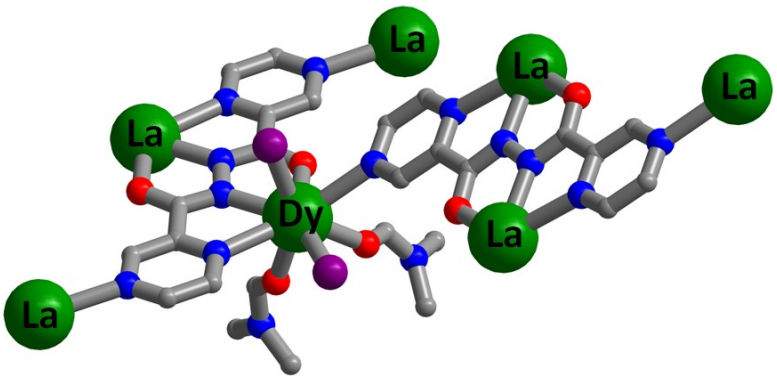

Figure S42. Extracted model structure of **1**; H atoms are omitted for clarify.

The basis sets for all atoms are atomic natural orbitals from the OpenMolcas ANO-RCC library: ANO-RCC-VTZP for Dy(III); VTZ for close Cl, O and N; VDZ for distant atoms. The calculations employed the second order Douglas-Kroll-Hess Hamiltonian, where scalar relativistic contractions were taken into account in the basis set and the spin-orbit couplings were handled separately in the restricted active space state interaction (RASSI-SO) procedure. Active electrons in 7 active orbitals include all *f* electrons (CAS (9 in 7) in the CASSCF calculation. To exclude all the

doubts, we calculated all the roots in the active space. We have mixed the maximum number of spin-free state which was possible with our hardware (all from 21 sextets, 128 from 224 quadruplets, 130 from 490 doublets for Dy(III) ion. SINGLE_ANISO program[S10-S12] was used to obtain the energy levels, ***g*** tensors, magnetic axes, *et al.* based on the above CASSCF/RASSI-SO calculations.

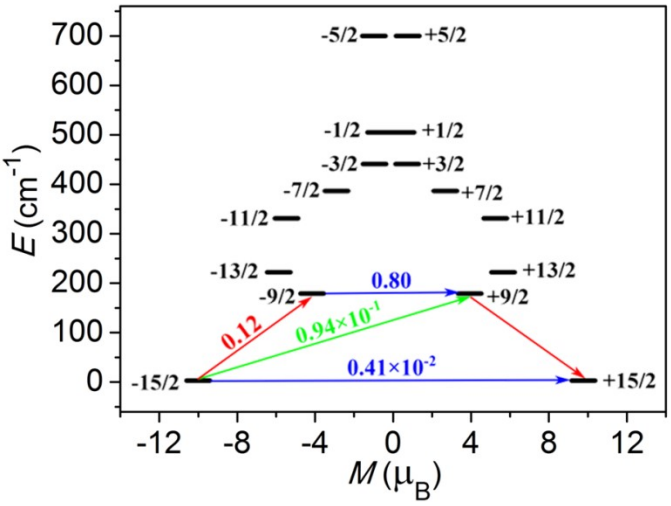

Figure S43. Magnetization blocking barrier of individual Dy(III) fragment of **[Dy]**. The thick black lines represent the KDs as a function of their magnetic moment along the magnetic axis. The blue lines correspond to diagonal quantum tunneling of magnetization (QTM); the green line represent off-diagonal relaxation process. The numbers at each arrow stand for the mean absolute value of the corresponding matrix element of transition magnetic moment.

Table S32 shows the energy levels, ***g*** (g_x, g_y, g_z) tensors and the predominant m_J values of the lowest eight Kramers doublets (KDs) of the individual Dy(III) ion. The ground state has strong anisotropic g tensors with $g_z \approx 20.000$, g_x, $g_y \approx 0.000$, indicating a perfect axial magnetic anisotropy of the individual Dy(III) ion.

To fit the exchange interaction in compound **1**, we took two steps to obtain it. Firstly, we calculated individual Dy(III) fragment using CASSCF/RASSI-SO to obtain the corresponding magnetic properties. Then, the exchange interaction between the magnetic centers was considered within the Lines model,[S13] while the account of

the dipole-dipole magnetic coupling was treated exactly. The Lines model is effective and has been successfully used widely in the research field of *d* and *f*-elements single-molecule magnets.[S14-S15]

For compound **1**, we only consider one type of $\hat{J}$ between the nearest Dy(III) ions. The Ising exchange Hamiltonian is: $\hat{J} = -2J\cos\theta$, where θ is an angle between the anisotropy axes on two Dy^{III} sites, and J is the Lines exchange coupling parameter. $\tilde{S}_{eff} = 1/2$ is the ground pseudospin on the Dy(III) site. $\hat{J}_{total}$ is the parameter of the total magnetic interaction ($\hat{J}_{total} = \hat{J}_{dip} + \hat{J}_{exch}$) between magnetic center ions. The dipolar magnetic coupling can be calculated exactly, while the exchange coupling constant was fitted through comparison of the computed and measured magnetic susceptibilities using POLY_ANISO program.[S10-S12]

We further provided the exchange energies, the energy differences between each exchange doublet Δ_t and main values of the g_z for the lowest two exchange doublets of individual Dy(III) fragment in Table S34, where the ground g_z value is 39.491, which also explains a ferromagnetic interaction in the [Dy_2] dimer. Because the main magnetic axes of the Dy(III) ion in the [Dy_2] dimer are parallel, the dimer can be regarded as a pseudospin $\tilde{S} = 1$.

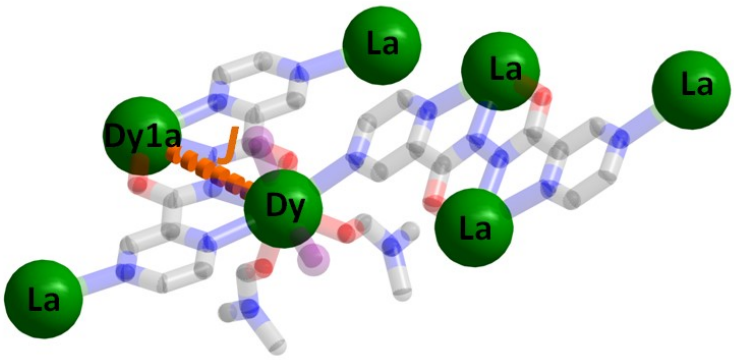

Figure S44. Scheme of the Dy^{III}-Dy^{III} interaction in compound **1**.

Table S32. Calculated energy levels (cm^{-1}), $\boldsymbol{g}$ (g_x, g_y, g_z) tensors and predominant m_J values of the lowest eight Kramers doublets (KDs) of individual Dy(III) fragment of **1** using CASSCF/RASSI-SO with OpenMolcas.

KDs	[Dy]			KDs	[Dy]			KDs	[Dy]		
	E (cm^{-1})	g	M_J		E (cm^{-1})	g	M_J		E (cm^{-1})	g	M_J
0	0.0	0.008	±15/2	**1**	174.0	0.581	±9/2	**2**	216.8	0.557	±13/2
		0.016				1.706				1.529	
		19.746				16.431				12.856	
3	324.4	1.308	±11/2	**4**	379.5	4.651	±7/2	**5**	433.3	0.813	±5/2
		3.040				5.264				1.201	
		11.379				10.993				12.956	
6	496.4	0.427	±1/2	**7**	689.8	0.008	±3/2				
		0.768				0.012					
		16.537				19.753					

Table S33. Wave functions with definite projection of the total moment | m_J > for the lowest eight KDs of individual Dy(III) fragment of **1**.

	E (cm^{-1})	wave functions
[Dy]	0.0	98.2%|±15/2>
	174.0	29.3%|±13/2>+11.1%|±7/2>+11.3%|±5/2>+14.7%|±3/2>+17.5%|±1/2>
	216.8	64.6%|±13/2>+9.4%|±5/2>+9.1%|±3/2>+9.1%|±1/2>
	324.4	72.1%|±11/2>+5.9%|±9/2>+5.5%|±3/2>
	379.5	14.9%|±11/2>+42.8%|±9/2>+19.5%|±7/2>+10.0%|±5/2>
	433.3	30.0%|±9/2>+29.5%|±7/2>+15.9%|±5/2>+14.1%|±1/2>
	496.4	21.3%|±7/2>+29.8%|±5/2>+25.7%|±3/2>+15.4%|±1/2>
	689.8	9.7%|±7/2>+19.2%|±5/2>+29.8%|±3/2>+36.7%|±1/2>

Table S34. Exchange energies E (cm^{-1}), the energy difference between each exchange doublets Δ_t (cm^{-1}) and the main values of the g_z for the lowest two exchange doublets of **1**.

	1		
	E	Δ_t	g_z
1	0.0000000000	9.174×10^{-7}	39.491
	0.0000009174		
2	0.2722980041	1.085×10^{-6}	0.000
	0.2722990895		

S6 REFERENCES

1. L. N. M. E. A. Boudreaux, Theory and Applications of Molecular Paramagnetism, John Wiley & Sons, New York, 1976.

2. SAINT Version 7.68A, Bruker AXS, Inc.; Madison, WI 2009.

3. G. M. Sheldrick, SADABS, Program for Empirical Absorption Correction of Area Detector Data. University of Göttingen, Germany, 1996.

4. G. M. Sheldrick, Crystal structure refinement with SHELXL, *Acta Crystallogr. Sect. C: Struct. Chem.*, 2015, **71**, 3–8.

5. I. F. Galván, M. Vacher, A. Alavi, C. Angeli, F. Aquilante, J. Autschbach, J. J. Bao, S. I. Bokarev, N. A. Bogdanov, R. K. Carlson, L. F. Chibotaru, J. Creutzberg, N. Dattani, M. G. Delcey, S. S. Dong, A. Dreuw, L. Freitag, L. M. Frutos, L. Gagliardi, F. Gendron, A. Giussani, L. González, G. Grell, M. Y. Guo, C. E. Hoyer, M. Johansson, S. Keller, S. Knecht, G. Kovacevic, E. Källman, G. L. Manni, M. Lundberg, Y. J. Ma, S. Mai, J. P. Malhado, P. Å. Malmqvist, P. Marquetand, S. A. Mewes, J. Norell, M. Olivucci, M. Oppel, Q. M. Phung, K. Pierloot, F. Plasser, M. Reiher, A. M. Sand, I. Schapiro, P. Sharma, C. J. Stein, L. K. Sørensen, D. G. Truhlar, M. Ugandi, L. Ungur, A. Valentini, S. Vancoillie, V. Veryazov, O. Weser, T. A. Wesołowski, Per-Olof. Widmark, S. Wouters, A. Zech, J. P. Zobel and R. Lindh, OpenMolcas: From Source Code to Insight, *J. Chem. Theory Comput.*, 2019, **15**, 5925–5964.

6. L. F. Chibotaru, L. Ungur and A. Soncini, The Origin of Nonmagnetic Kramers Doublets in the Ground State of Dysprosium Triangles: Evidence for a Toroidal Magnetic Moment, *Angew. Chem., Int. Ed.*, 2008, **47**, 4126–4129.

7. L. Ungur, W. Van den Heuvel and L. F. Chibotaru, Ab initio investigation of the non-collinear magnetic structure and the lowest magnetic excitations in dysprosium triangles, *New J. Chem.*, 2009, **33**, 1224–1230.

8. L. F. Chibotaru, L. Ungur, C. Aronica, H. Elmoll, G. Pilet and D. Luneau, Structure, Magnetism, and Theoretical Study of a Mixed-Valence $Co^{II}_3Co^{III}_4$ Heptanuclear Wheel: Lack of SMM Behavior despite Negative Magnetic Anisotropy, *J. Am. Chem. Soc.*, 2008, **130**, 12445–12455.

9. M. E. Lines, Orbital Angular Momentum in the Theory of Paramagnetic Clusters, *J. Chem. Phys*., 1971, **55**, 2977–2984.

10. K. C. Mondal, A. Sundt, Y. H. Lan, G. E. Kostakis, O. Waldmann, L. Ungur, L. F. Chibotaru, C. E. Anson and A. K. Powell, Coexistence of Distinct Single-Ion and Exchange-Based Mechanisms for Blocking of Magnetization in a $Co^{II}_2Dy^{III}_2$ Single-Molecule Magnet, *Angew. Chem., Int. Ed*., 2012, **51**, 7550–7554.

11. S. K. Langley, D. P. Wielechowski, V. Vieru, N. F. Chilton, B. Moubaraki, B. F. Abrahams, L. F. Chibotaru and K. S. Murray, A {($Cr_2^{III}Dy_2^{III}$)} Single-Molecule Magnet: Enhancing the Blocking Temperature through 3d Magnetic Exchange, *Angew. Chem., Int. Ed*., 2013, **52**, 12014–12019.

12. M. Pinsky and D. Avnir, Continuous Symmetry Measures. 5. The Classical Polyhedra, *Inorg. Chem.*, 1998, **37**, 5575–5582.

13. D. Matoga, J. Szklarzewicz, K. Stadnicka and M. S. Shongwe, Iron(III) Compounds with a Biologically Relevant Aroylhydrazone: Crystallographic Evidence for Coordination Versatility, *Inorg. Chem.*, 2007, **46**, 9042-9044.

14. S. Demir, I. R. Jeon, J. R. Long and T. D. Harris, Radical ligand-containing single-molecule magnets, *Coord. Chem. Rev.*, 2015, **289−290**, 149−176.

15. B. S. Dolinar, D. I. Alexandropoulos, K. R. Vignesh, T. James and K. R. Dunbar, Lanthanide Triangles Supported by Radical Bridging Ligands, *J. Am. Chem. Soc.*, 2018, **140**, 908–911.

16. L. Liu, X. Ren, J. H. Xie, B. Cheng, W. K. Liu, T. Y. An, H. W. Qin and J. F. Hu, Magnetic switches via electric field in BN nanoribbons, *Appl. Surf. Sci.*, 2019, **480**, 300–307.